A&A 541, A115 (2012)
DOI: 10.1051/0004-6361/201118742

Astronomy & Astrophysics

VLT/X-shooter observations of blue compact galaxies Haro 11 and ESO 338-IG 004⋆,⋆⋆

N. G. Guseva[1,2], Y. I. Izotov[1,2], K. J. Fricke[1,3], and C. Henkel[1,4]

[1] Max-Planck-Institut für Radioastronomie, Auf dem Hügel 69, 53121 Bonn, Germany
e-mail: guseva@mao.kiev.ua
[2] Main Astronomical Observatory, Ukrainian National Academy of Sciences, Zabolotnoho 27, Kyiv 03680, Ukraine
[3] Institut für Astrophysik, Göttingen Universität, Friedrich-Hund-Platz 1, 37077 Göttingen, Germany
[4] Astronomy Department, King Abdulaziz University, PO Box 80203, Jeddah, Saudi Arabia

Received 25 December 2011 / Accepted 28 February 2012

ABSTRACT

Context. Strongly star-forming galaxies of subsolar metallicities are typical of the high-redshift universe. Here we therefore provide accurate data for two low-z analogs, the well-known low-metallicity emission-line galaxies Haro 11 and ESO 338-IG 004.
Aims. Our main goal is to derive their spectroscopic properties and to examine whether a previously reported near-infrared (NIR) excess in Haro 11 can be confirmed.
Methods. On the basis of Very Large Telescope/X-shooter spectroscopic observations in the wavelength range $\sim\lambda\lambda$3000–24 000 Å, we use standard direct methods to derive physical conditions and element abundances. Furthermore, we use X-shooter data together with *Spitzer* observations in the mid-infrared range to attempt to find hidden star formation.
Results. We derive interstellar oxygen abundances of 12 + log O/H = 8.33 ± 0.01, 8.10 ± 0.04, and 7.89 ± 0.01 in the two H II regions B and C of Haro 11 and in ESO 338-IG 004, respectively. The observed fluxes of the hydrogen lines correspond to the theoretical recombination values after correction for extinction with a single value of the extinction coefficient $C(\mathrm{H}\beta)$ across the entire wavelength range from the near-ultraviolet to the NIR and mid-infrared for each of the studied H II regions. Thus, we confirm our previous findings obtained for several low-metallicity emission-line galaxies (Mrk 59, II Zw 40, Mrk 71, Mrk 996, SBS 0335–052E, PHL 293B, and GRB HG 031203) that the extinction coefficient $C(\mathrm{H}\beta)$ is not higher in the NIR than in the optical range and therefore that there are no emission-line regions contributing to the line emission in the NIR range, which are hidden in the optical range. The agreement between the extinction-corrected and CLOUDY-predicted fluxes implies that a H II region model including only stellar photoionisation is able to account for the observed fluxes, in both the optical and NIR ranges. No additional excitation mechanism such as shocks from stellar winds and supernova remnants is needed. All observed spectral energy distributions (SEDs) can be reproduced quite well across the whole wavelength range by model SEDs except for Haro 11B, where there is a continuum flux excess at wavelengths >1.6 μm. It is possible that one or more red supergiant stars are responsible for the NIR flux excess in Haro 11B. We find evidence of a luminous blue variable (LBV) star in Haro 11C.

Key words. galaxies: fundamental parameters – galaxies: starburst – galaxies: ISM – galaxies: abundances – stars: activity

1. Introduction

Haro 11 (≡ESO 0350-IG 038) and ESO 338-IG 004 (≡Tololo 1924–416) are prominent blue compact galaxies (BCG) with $M_B = -20.0$ mag and −18.9 mag, respectively (Bergvall & Östlin 2002). Both exhibit perturbed morphologies, high star-formation rates (SFRs), and multiple-component Hα velocities fields reflecting signatures of merger events (Östlin et al. 2001).

Haro 11 is a massive and luminous BCG with a SFR ∼ 18–20 $M_\odot$ yr^{-1} (Bergvall & Östlin 2002) which possesses multiple H II regions, called A, B, and C following the nomenclature of Kunth et al. (2003). Östlin et al. (2001) estimated that the stellar mass of the galaxy is 10^{10} $M_\odot$ from the Hα velocity field, while Bergvall et al. (2000) derived a total gas mass of 2×10^9 $M_\odot$. The high present SFR of 22 ± 3 $M_\odot$ yr^{-1} in Haro 11 was derived by Adamo et al. (2010). The galaxy is a Lyα and Ly-continuum emitter (Hayes et al. 2007) and also a luminous IRAS source (Bergvall et al. 2000) with an IR luminosity of 1.9×10^{11} $L_\odot$, which is a characteristic property of luminous IR galaxies (LIRGs). High star-formation activity in Haro 11 and its global properties are similar to those in high-redshift Lyman break galaxies (LBGs) at $z\sim3$ (Pettini et al. 2001) and those in lower-redshift luminous compact emission-line galaxies (LCGs) from SDSS DR7 (Izotov et al. 2011a) and in green pea galaxies (Cardamone et al. 2009).

ESO 338-IG 004 contains two H II regions in its most active part, which is referred to its "centre" and "H II region" (Bergvall 1985; Bergvall & Östlin 2002). The central starburst ("centre") of the galaxy is resolved by *Hubble* Space Telescope (HST) images into compact star clusters (Meurer et al. 1995; Östlin et al. 1998) and young globular clusters (Östlin et al. 1998). Bergvall (1985) estimated the dynamical mass of the galaxy, $M_{\rm tot}\sim1\times10^9$ $M_\odot$. Östlin et al. (2007) derived the dynamical mass $M = 1.3\times10^7$ $M_\odot$ and an age of ∼6 Myr for the brightest cluster #23 in ESO 338-IG 004 from an analysis of the absorption components of Hδ and H8 – H11 Balmer lines.

Bergvall & Östlin (2002) obtained a very red colour $V-K = 4.2\pm0.8$ mag for a Haro 11 underlying LSB component. On the

⋆ Based on observations collected at the European Southern Observatory, Chile, ESO programme 60.A-9433(A).
⋆⋆ Figures 1–3 and Table 1 are available in electronic form at http://www.aanda.org

other hand, Micheva et al. (2010) derived a far less red $V - K$ colour of the Haro 11 LSB component of 2.3 ± 0.2 mag from new deep V and K photometry. On the basis of high-resolution HST imaging of Haro 11 in eight wavelength bands from the ultraviolet (UV) to K, Adamo et al. (2010) found about 100 star clusters with flux excesses at wavelengths >8000 Å with respect to the synthetic evolutionary models. This is almost half of the whole cluster sample in Haro 11. Moreover, both of the giant H II regions of Haro 11B and C are very massive ($\sim 1 \times 10^7$ $M_\odot$) and have a red excess.

Based on ESO 3.6 m telescope observations, Bergvall (1985) obtained an oxygen abundance of 12 + log O/H = 8.08 for the central $3'' \times 4''$ region of ESO 338-IG 004 by applying the direct T_e-method with the use of the emission line [O III]λ4363 Å. An oxygen abundance 12 + log O/H = 7.92, which was derived using the T_e-method, was obtained by Masegosa et al. (1994) and Raimann et al. (2000) from the same spectra acquired by Terlevich et al. (1991).

Finally, Bergvall & Östlin (2002) using ESO 1.5-m and 3.6-m spectra (obtained in 1983, 1984 and 1986) derived 12 + log O/H = 7.9 and 8.0 for Haro 11 and ESO 338-IG 004, respectively, again using the T_e-method.

We note, however, that in the case of Haro 11, such a fundamental parameter as the metallicity remains uncertain despite of many previous comprehensive studies. This is because the important [O III]λ4363 Å line is blended with the [Fe II]λ4359 Å line (this paper) and therefore an accurate measurement of the former line's flux was impossible with previous low-spectral-resolution observations.

We present here high-quality archival Very Large Telescope (VLT)/X-shooter spectroscopic observations of the two bright knots B and C in Haro 11 and of the brightest part of ESO 338-IG 004 over a wide wavelength range ~λ3000–24 000 Å. These new medium-spectral-resolution observations allow us to more accurately derive reddening, the physical conditions, and the element abundances in the H II regions. Moreover, since cool low-mass stars are a main contributor to the stellar mass and they emit mainly in the near-infrared (NIR) range, observations of a very broad wavelength range permit us to derive more reliable stellar masses for the galaxies and their specific SFRs. The observations from the UV to NIR wavelength ranges also allow us to study whether any hidden star formation is present in these galaxies. We note, however, that in low-metallicity compact galaxies with high SFRs the strongly ionised gaseous emission contributes to the total spectral energy distribution (SED) and therefore should be properly taken into account for the stellar mass determination.

Thus, the main goals of this paper are to obtain more accurate element abundances, to test spectroscopically the flux excess in the NIR wavelength range found by Adamo et al. (2010) for Haro 11B and C, to search for star formation seen in the NIR range but hidden in the optical range, and to estimate the excitation mechanisms of bright emission lines using additionally the *Spitzer* observations of Wu et al. (2008) in the mid-infrared (MIR) range.

In Sect. 2, we describe the observations and data reduction. We present the main properties of the galaxies in Sect. 3. More specifically, the element abundances are presented in Sect. 3.1, the hidden star formation is discussed in Sect. 3.2, the H_2 emission is considered in Sect. 3.3, the CLOUDY modelling is discussed in Sect. 3.4, the possible presence of LBV stars in Haro 11C and Haro 11B in Sect. 3.5, and the SED fitting is described in Sect. 3.6. Finally, in Sect. 4 we summarize our main results.

2. Observations

New spectra of the blue compact emission-line galaxies Haro 11 and ESO 338-IG 004 were obtained with the VLT/X-shooter on 2009 August 11 and 12, respectively [ESO program 60.A-9433(A)].

The observations were performed in the wavelength range ~λ3000–24 000 Å using the three-arm echelle X-shooter spectrograph mounted at the UT2 Cassegrain focus. All observations were obtained at low airmass 1.016, 1.012, and 1.430 for Haro 11B, Haro 11C, and ESO 338-IG 004, respectively, thus the effect of the atmospheric dispersion was low. The seeings were 0.″72–0.″75, 0.″70–1.″32, and 0.″61–0.″66 for Haro 11B, C, and ESO 338-IG 004 observations, respectively. For each of the UVB, VIS, and NIR arms, the total exposure times were 800s, 680s, and 600s for Haro 11B, Haro 11C, and ESO 338-IG 004, respectively. They were broken into two equal subexposures. The nodding along the slit was performed according to the scheme AB with the object positions A or B differing by 4″ along the slit for each H II region. In the UVB arm with wavelength range ~λ3000–5600 Å, a slit of $1'' \times 11''$ was used. In the VIS and NIR arms with wavelength ranges ~λ5500–10 200 Å and ~λ10 200–24 000 Å, respectively, slits of $0.''9 \times 11''$ were used. The binning factors in the UVB and VIS arms along the spatial and dispersion axes were 1 and 2, respectively, while in the NIR arm they were 1 and 1. Resolving powers $\lambda/\Delta\lambda$ of 5100, 8800, and 5100 characterise the UVB, VIS, and NIR arms, respectively. Spectra of thorium-argon (Th-Ar) comparison arcs were used to perform the wavelength calibration of the UVB and VIS arm observations. For the wavelength calibration of the NIR spectrum, we used night sky emission lines.

The two-dimensional UVB and VIS spectra were bias subtracted and flat-field corrected using IRAF[1]. The NIR dark current frames were subtracted from the NIR flat frames. The two-dimensional NIR spectra of objects were then divided by the flat frames to correct for the pixel sensitivity variations. Cosmic ray hits of all UVB, VIS, and NIR spectra were removed using the routine CRMEDIAN. The remaining hits were later removed manually after background subtraction.

For each of the UVB, VIS, and NIR arms, the spectrum at the position B was subtracted from the spectrum at the position A. This resulted in a frame with subtracted background. We used the IRAF software routines IDENTIFY, REIDENTIFY, FITCOORD, and TRANSFORM to perform wavelength calibration and correct for distortion and tilt for each frame. The one-dimensional wavelength-calibrated spectra were then extracted from the two-dimensional frames using the APALL routine. We adopted extraction apertures of $1'' \times 4''$, $0.''9 \times 4''$, and $0.''9 \times 4''$ for the UVB, VIS, and NIR spectra, respectively. Before extraction, the spectra at the positions A and B in the two-dimensional background-subtracted frames were carefully aligned with the routine ROTATE and co-added. The spectrophotometric standard star Feige 110 was used to perform the flux calibration. Its spectra in all arms were obtained with a wide slit of $5'' \times 11''$.

The resulting flux-calibrated and redshift-corrected UVB, VIS, and NIR spectra of Haro 11B, C, and ESO 338-IG 004 are shown in Figs. 1–3.

[1] IRAF is the Image Reduction and Analysis Facility distributed by the National Optical Astronomy Observatory, which is operated by the Association of Universities for Research in Astronomy (AURA) under cooperative agreement with the National Science Foundation (NSF).

3. Results

3.1. Element abundances

We derived element abundances from emission-line fluxes using a classical semi-empirical method. The fluxes in all spectra were measured using the IRAF SPLOT routine. The line flux errors include statistical errors derived with SPLOT from non-flux-calibrated spectra, in addition to errors introduced by the absolute flux calibration, which we set to 1% of the line fluxes, according to the uncertainties in the absolute fluxes of relatively bright standard stars (Oke 1990; Colina & Bohlin 1994; Bohlin 1996; Izotov & Thuan 2004). These errors were propagated into the calculation of the electron temperatures, the electron number densities, and the ionic and total element abundances following the prescription of Guseva et al. (2011b).

The extinction coefficient $C(\mathrm{H}\beta)$ and equivalent widths of the hydrogen absorption lines EW(abs) are calculated by simultaneously minimising the deviations in the corrected fluxes $I(\lambda)/I(\mathrm{H}\beta)$ of all hydrogen Balmer lines from their theoretical recombination values. The fluxes were corrected for both extinction, using the reddening curve of Cardelli et al. (1989), and underlying hydrogen stellar absorption (Izotov et al. 1994). The derived $C(\mathrm{H}\beta)$ was applied to correct all emission-line fluxes in the entire wavelength range $\lambda\lambda$3000–24 000 Å. The extinction-corrected relative fluxes $I(\lambda)/I(\mathrm{H}\beta) \times 100$ of the lines, the extinction coefficient $C(\mathrm{H}\beta)$, the equivalent width of the Hβ emission line $EW(\mathrm{H}\beta)$, the Hβ observed flux $F(\mathrm{H}\beta)$, and the equivalent width of the underlying hydrogen absorption lines EW(abs) are given in Table 1 (available only in the online edition). We note that the fluxes of the Balmer hydrogen emission lines corrected for extinction and underlying hydrogen absorption (Cols. 3, 5, and 7 in Table 1) are close to the theoretical recombination values of Hummer & Storey (1987) (Col. 8 of the Table 1), suggesting that the extinction coefficient $C(\mathrm{H}\beta)$ is reliably derived.

The physical conditions, and the ionic and total heavy element abundances in the ISM of the galaxies were derived following Izotov et al. (2006) (Table 2). In particular, applying the direct T_e-method, we derived the electron temperature T_e(O III) from the [O III] λ4363/(λ4959 + λ5007) emission-line ratio. The electron temperatures T_e(O II) and T_e(S III) were derived from the empirical relations based on the photoionisation models of H II regions (Izotov et al. 2006). The electron number densities N_e(S II) were obtained from the [S II]λ6717/λ6731 emission-line ratios. The electron temperatures T_e(O III), T_e(O II), and T_e(S III), the electron number densities N_e(S II), the ionisation correction factors ICFs, and the ionic and total O, N, Ne, S, Ar, Fe, and Cl abundances derived from the forbidden emission lines are given in Table 2.

We derive $12 + \log \mathrm{O/H} = 8.33 \pm 0.01$ and 8.10 ± 0.04 for Haro 11B and C, respectively, which is appreciably higher than the oxygen abundance $12 + \log \mathrm{O/H} = 7.9$ obtained by Bergvall & Östlin (2002) in an aperture $4'' \times 4''$ for the brightest region of Haro 11. We also obtain a higher extinction $C(\mathrm{H}\beta) = 0.74$ for Haro 11B than $C(\mathrm{H}\beta) = 0.27$ for Haro 11C. It can indeed be seen in the HST images obtained by Adamo et al. (2010) that Haro 11B is more obscured by dust clouds than Haro 11C. Adamo et al. (2010) also derived different extinctions of $E(B-V) = 0.38$ and 0.06 (or $C(\mathrm{H}\beta) = 0.56$ and 0.09) for Haro 11B and Haro 11C, respectively. For comparison, Hayes et al. (2007) derived $E(B-V) = 0.42$ and 0.48 (or $C(\mathrm{H}\beta) = 0.62$ and 0.70) and Vader et al. (1993) derived $E(B-V) = 0.41$ and 0.39 for Haro 11B and C, respectively.

Table 2. Physical conditions and element abundances.

Galaxy	Haro 11B	Haro 11C	ESO 338-IG 004
Property		Value	
T_e(O III), K	10144 ± 70	11362 ± 449	14771 ± 137
T_e(O II), K	10099 ± 77	11552 ± 500	13786 ± 160
T_e(S III), K	10110 ± 58	11209 ± 373	14397 ± 114
N_e(S II), cm^{-3}	10 ± 10	10 ± 10	142 ± 36
O^+/H^+, ($\times 10^5$)	8.38 ± 0.28	5.21 ± 0.76	1.66 ± 0.06
O^{2+}/H^+, ($\times 10^5$)	12.78 ± 0.33	7.48 ± 0.91	5.87 ± 0.16
O^{3+}/H^+, ($\times 10^5$)	0.22 ± 0.02	...	0.19 ± 0.01
O/H, ($\times 10^5$)	21.38 ± 0.43	12.69 ± 1.19	7.73 ± 0.17
12+log O/H	8.33 ± 0.01	8.10 ± 0.04	7.89 ± 0.01
N^+/H^+, ($\times 10^6$)	8.87 ± 0.29	7.48 ± 1.13	0.62 ± 0.03
ICF(N)[a]	2.93	2.72	4.54
N/H, ($\times 10^6$)	25.99 ± 1.06	20.37 ± 3.94	2.82 ± 0.16
log N/O	–0.92 ± 0.02	–0.79 ± 0.09	–1.44 ± 0.03
Ne^{2+}/H^+, ($\times 10^5$)	3.10 ± 0.09	2.09 ± 0.28	1.34 ± 0.04
ICF(Ne)[a]	1.49	1.42	1.13
Ne/H, ($\times 10^5$)	4.62 ± 0.17	2.97 ± 0.49	1.52 ± 0.05
log Ne/O	–0.66 ± 0.02	–0.63 ± 0.08	–0.71 ± 0.02
S^+/H^+, ($\times 10^6$)	0.57 ± 0.01	0.68 ± 0.06	0.22 ± 0.01
S^{2+}/H^+, ($\times 10^6$)	2.39 ± 0.08	1.48 ± 0.31	0.77 ± 0.04
ICF(S)[a]	1.07	1.06	1.23
S/H, ($\times 10^6$)	3.17 ± 0.10	2.29 ± 0.35	1.22 ± 0.05
log S/O	–1.83 ± 0.02	–1.74 ± 0.08	–1.80 ± 0.02
Ar^{2+}/H^+, ($\times 10^7$)	6.23 ± 0.14	5.59 ± 0.44	2.42 ± 0.06
Ar^{3+}/H^+, ($\times 10^7$)	0.58 ± 0.05	...	0.89 ± 0.07
ICF(Ar)[a]	1.07	1.08	1.11
Ar/H, ($\times 10^7$)	6.69 ± 0.16	6.02 ± 0.52	2.69 ± 0.11
log Ar/O	–2.50 ± 0.01	–2.32 ± 0.06	–2.46 ± 0.02
[Fe III] λ4658:			
Fe^{2+}/H^+, ($\times 10^6$)	0.99 ± 0.03	1.32 ± 0.17	0.24 ± 0.01
ICF(Fe)[a]	3.73	3.48	6.17
Fe/H, ($\times 10^6$)	3.69 ± 0.16	4.61 ± 0.88	1.49 ± 0.10
log Fe/O	–1.76 ± 0.02	–1.44 ± 0.09	–1.71 ± 0.03
[Fe III] λ4986:			
Fe^{2+}/H^+, ($\times 10^6$)	0.35 ± 0.02	0.51 ± 0.09	0.29 ± 0.01
ICF(Fe)[a]	3.73	3.48	6.17
Fe/H, ($\times 10^6$)	1.30 ± 0.07	1.78 ± 0.42	1.77 ± 0.11
log Fe/O	–2.21 ± 0.02	–1.85 ± 0.11	–1.64 ± 0.03
Cl^{2+}/H^+, ($\times 10^7$)	0.35 ± 0.02	0.71 ± 0.12	...
ICF(Cl)[a]	1.13	1.17	...
Cl/H, ($\times 10^7$)	0.39 ± 0.02	0.84 ± 0.23	...
log Cl/O	–3.73 ± 0.03	–3.18 ± 0.13	...

Notes. [(a)] Ionisation correction factor.

The differences in oxygen abundance of Haro 11 are likely not solely due to differences in the extinction but may also be caused by blending of the [O III]λ4363 Å emission line with the [Fe II]λ4359 Å one in previous low-spectral-resolution observations. The higher-spectral-resolution X-shooter observations have allowed to resolve this blend. In Table 1 we can clearly see, that the fluxes of the [Fe II]λ4359 Å emission line in Haro 11B and Haro 11C are, respectively, 27% and 151% of the [O III]λ4363 Å emission-line fluxes.

The oxygen abundance 12+logO/H = 7.89 ± 0.01 of ESO 338-IG 004 is slightly lower than the previous determinations

Table 3. Stellar masses and ages of young stellar populations.

ID	Mass ($M_\odot$)	Age (Myr)	$C(\mathrm{H}\beta)$
	This paper[a]		
Haro 11B	1.26×10^8	2.9	0.74
Haro 11C	2.05×10^8	4.2	0.27
ESO 338-IG 004	0.56×10^8	1.9	0.37
	Adamo et al. (2010)[b]		
Haro 11B	8.35×10^6	3.5	0.56
Haro 11C	1.36×10^7	9.5	0.09
	Östlin et al. (2007)[c]		
ESO 338-IG 004	1.3×10^7	6.3	...

Notes. [(a)] VLT/X-shooter data. [(b)] HST photometric data. [(c)] VLT/UVES data for the brightest cluster #23.

of 12 + log O/H = 7.92 (Masegosa et al. 1994; Raimann et al. 2000), 8.08 (Bergvall 1985), 8.0 (Bergvall & Östlin 2002) and 7.99 (Guseva et al. 2011a), where the direct T_e-method was also used. We note that our determination of $C(\mathrm{H}\beta) = 0.31$ (see Table 1) is larger than the $C(\mathrm{H}\beta)$ in the range 0.0–0.05 derived by Bergvall (1985), Raimann et al. (2000), and Guseva et al. (2011a), and $E(B-V) < 0.1$ of Bergvall & Östlin (2002). From the fits of model SEDs to the SEDs derived from HST images with different filters, Östlin et al. (2009) derived a low value of $C(\mathrm{H}\beta) \sim 0.1$ for ESO 338-IG 004. These differences may be caused by the oxygen abundances having been derived by different authors for different regions in ESO 338-IG 004. To check this possibility, we extracted separate spectra in addition to the integrated spectrum, for the "centre" and "H II region". For the centre, we derived 12+log O/H = 7.82 ± 0.01, which is lower than that for the integrated spectrum, but for the H II region we obtain a higher value of 8.00 ± 0.01, which is more consistent with some of the previous observations.

The abundance ratios of the different species log N/O, log Ne/O, log S/O, log Ar/O, log Fe/O, and log Cl/O (Table 2) obtained for Haro 11B, C, and ESO 338-IG 004 are in the range of the ratios obtained for different samples of blue compact galaxies, such as the HeBCD sample of Izotov et al. (2004) and Izotov & Thuan (2004) used to determine the primordial He abundance (consisting of more than 100 emission-line galaxies), the sample of ~300 emission-line galaxies from the SDSS DR3 of Izotov et al. (2006), and the VLT sample of 121 low-metallicity emission-line galaxies studied by Guseva et al. (2011a). The high values of log N/O in Haro 11B (−0.92, Table 2) and in Haro 11C (−0.79) agree with the value of log N/O = −0.7 derived by Bergvall & Östlin (2002) for Haro 11. Our values of log N/O, log Ne/O, and log S/O for ESO 338-IG 004 (Table 2) are consistent with the data of Masegosa et al. (1994) (log N/O = −1.40 ± 0.01 and log Ne/O = −0.75 ± 0.10), Raimann et al. (2000) (log N/O = −1.57), Bergvall (1985) (log N/O = −1.18, and log S/O = −1.63), Bergvall & Östlin (2002) (log N/O = −1.5), and Guseva et al. (2011a) (log N/O = −1.34, log Ne/O = −0.78, and log S/O = −1.60).

3.2. Hidden star formation

The spectra of the studied galaxies were obtained simultaneously over the entire optical and near-infrared wavelength ranges. This enables us to directly compare the extinctions derived for the optical and NIR spectra.

The observed $F(\lambda)$ and extinction-corrected $I(\lambda)$ fluxes of the emission lines, and the extinction coefficients $C(\mathrm{H}\beta)$ are shown in Table 1. The extinction coefficients $C(\mathrm{H}\beta) = 0.74$, 0.27, and 0.31 for Haro 11B, C, and ESO 338-IG 004, respectively, are derived from the hydrogen Balmer lines only in the UVB and VIS arm spectra. They are adopted for the correction of emission-line fluxes not only in the UVB and VIS spectra, but also in the NIR range. We also show in Table 1 the theoretical recombination fluxes for hydrogen Balmer, Paschen, and Brackett lines calculated by Hummer & Storey (1987) (last column of the Table), adopting a case B model with an electron temperature $T_e = 12\,500$ K, and an electron number density $N_e = 100$ cm^{-3}.

The deviations of the observed fluxes of bright Balmer, Paschen and Brackett hydrogen lines after correction for extinction with a single value of $C(\mathrm{H}\beta)$ from the theoretical recombination values (Hummer & Storey 1987) do not exceed a few percent (cf. Table 1). The exceptions are extinction-corrected fluxes of several Paschen and Brackett hydrogen lines marked in Table 1, which deviate significantly from the theoretical values (e.g., Paβ line) because of strong telluric absorption. Excluding these lines, we may conclude that a single $C(\mathrm{H}\beta)$ value derived from the hydrogen Balmer lines can be used over the entire wavelength range of $\sim\lambda\lambda$3000–24 000 Å.

Thus, we confirm our previous findings obtained for several low-metallicity emission-line galaxies (Mrk 59, II Zw 40, Mrk 71, Mrk 996, SBS 0335–052E, PHL 293B, and GRB HG 031203) that the extinction coefficient $C(\mathrm{H}\beta)$ is not systematically higher across the NIR wavelength range than the optical range and that no additional regions contribute to the NIR line emission that are, however, hidden in the optical range (Vanzi et al. 2000, 2002; Izotov et al. 2009, 2011b; Izotov & Thuan 2011; Guseva et al. 2011b).

3.3. H_2 ro-vibrational emission

Molecular hydrogen lines do not originate in H II regions, but in neutral molecular clouds. In the NIR, they are excited by two mechanisms. The first is a thermal mechanism consisting of collisions between neutral species (e.g., H, H_2), resulting from large-scale shocks driven by powerful stellar winds, supernova (SN) remnants, or molecular cloud-cloud collisions. The second is fluorescence due to the absorption of ultraviolet photons produced by hot stars. By comparing the observed line ratios with those predicted by for instance the models of Black & Dishoeck (1987), it is possible to discriminate between the two processes. In particular, line emission from the vibrational level $v = 2$ and higher vibrational levels are virtually absent in collisionally excited spectra, while they are relatively strong in fluorescent spectra.

Thirteen ro-vibrational H_2 emission lines are detected in the NIR spectrum of Haro 11B (see Fig. 1). Only two H_2 emission lines, 1.957 μm 1–0 $S(3)$ and 2.122 μm 1–0 $S(1)$, are detected in the spectrum of ESO 338-IG 004 and no H_2 lines are detected in the spectrum of Haro 11C (Table 1). The fluxes of the H_2 lines relative to that of the strongest 2.122 μm 1–0 $S(1)$ line are shown in Table 4. Two H_2 emission lines, the 1.188 μm 2–0 $S(0)$ and the 1.238 μm 2–0 $Q(1)$ transitions are blended with the Fe II lines. The very large observed flux ratio of the 1.188 μm line (Table 4) can be due to contamination by a singly ionised iron line. The last two columns show the theoretical ratios calculated by Black & Dishoeck (1987) in the cases of fluorescent and collisional excitation. It can be seen that the observed line flux ratios for most of the H_2 lines agree with those predicted for fluorescent

Table 4. H_2 emission line flux ratios for Haro 11B.

λ	Line	Observations[a]	Model[b]	
μm			Fluor.	Collis.
1.162	H_2 2–1 $S(1)$	0.2	0.4	0.0
1.185	H_2 3–1 $S(3)$	0.2	0.4[c]	...
1.188	H_2 2–0 $S(0)$+[Fe II]	0.9	0.2[c]	...
1.207	H_2 3–1 $S(2)$	0.1	0.2	0.0
1.233	H_2 3–1 $S(1)$	0.6	0.5	0.0
1.238	H_2 2–0 $Q(1)$+Fe II?	0.2	0.4	0.0
1.601	H_2 6–4 $Q(1)$	0.1	0.4	0.0
1.957	H_2 1–0 $S(3)$	0.5	0.7[c]	...
2.034	H_2 1–0 $S(2)$	0.3	0.5	0.3
2.073	H_2 2–1 $S(3)$	0.3	0.2	0.0
2.122	H_2 1–0 $S(1)$	1.0	1.0	1.0
2.223	H_2 1–0 $S(0)$	0.2	0.6	0.3
2.248	H_2 2–1 $S(1)$	0.2	0.5	0.0

Notes. [(a)] Flux ratios relative to the H_2 2.122 μm flux. [(b)] Model values by Black & Dishoeck (1987). We adopt their model 1 for fluorescent lines and model S1 for collisionally excited lines. [(c)] Flux ratios are from model 14 by Black & Dishoeck (1987), because these lines are not present in model 1.

Table 5. Input parameters for the CLOUDY model.

Parameter	Haro 11B	Haro 11C
log Q(H)[a]	53.51	52.30
Starburst age, log Myr	6.35	6.50
N_e, cm^{-3}	10	10
f[b]	0.02	0.06
log He/H	–0.93	–0.93
log C/H	–3.97	–4.20
log N/H	–4.58	–4.69
log O/H	–3.67	–3.90
log Ne/H	–4.33	–4.53
log S/H	–5.50	–5.64
log Ar/H	–6.17	–6.22

Notes. [(a)] Q(H) is the number of ionising photons per second. [(b)] Volume filling factor.

excitation, supporting the previous findings that fluorescence is the main excitation mechanism of ro-vibrational H_2 lines in most BCDs with high-excitation H II regions (Vanzi et al. 2000, 2008; Izotov et al. 2009; Izotov & Thuan 2011). However, there are still some BCDs (e.g., PHL 293B Izotov et al. 2011b) for which the collisional excitation of ro-vibrational H_2 lines is the dominat excitation.

3.4. CLOUDY models

Using the CLOUDY code (version c10.00) of Ferland et al. (1998), we examine the excitation mechanisms not only of the hydrogen lines but all emission lines by producing stellar photoionisation models for our objects. The CLOUDY input parameters for the best-fit models with a single stellar population are shown in Table 5. The logarithm of the number of ionising photons per second Q(H) is calculated from the extinction-corrected Hβ luminosity. We adopt the shape of the ionising stellar radiation of the Starburst-99 models (Leitherer et al. 1999) with a starburst age shown in Table 5. The electron number density N_e is assumed to be constant with radius. The ratios of abundances of different species to hydrogen are taken from this paper, except for carbon which has no bright emission lines in the optical and NIR ranges. To obtain the abundance of this species, we use a relation C/O vs. oxygen abundance for the emission-line galaxies studied by Garnett et al. (1995). The emission-line fluxes for the best-fit models are shown in Table 6.

Table 6. Comparison of the observed and predicted intensities of some strong emission lines in Haro 11B and C.

Ion	CLOUDY		Observations[a]	
	B[b]	C[b]	B[b]	C[b]
	I/I(Hβ)	I/I(Hβ)	I/I(Hβ)	I/I(Hβ)
3727 [O II][c]	2.058	1.927	2.186	2.336
3869 [Ne III]	0.283	0.321	0.299	0.314
4101 Hδ	0.264	0.267	0.277	0.269
4340 Hγ	0.472	0.475	0.499	0.461
4861 Hβ	1.000	1.000	1.000	1.000
4959 [O III]	1.208	1.070	1.194	0.990
5007 [O III]	3.635	3.220	3.716	3.172
6563 Hα	2.917	2.891	2.907	2.864
6583 [N II]	0.342	0.381	0.488	0.576
6716 [S II]	0.072	0.078	0.156	0.291
6731 [S II]	0.051	0.055	0.102	0.134
9069 [S III]	0.172	0.154	0.156	0.144
9532 [S III]	0.426	0.382	0.432	0.385
10 829 He I	0.286	0.254	0.326	0.283
12 570 [Fe II]	0.021	0.030	0.014	0.028
12 821 Paβ	0.164	0.161	0.144	0.176
16 436 [Fe II]	0.018	0.025	0.012	0.017
19 450 Brδ	0.018	0.018	0.019	0.014
21 661 Brγ	0.028	0.027	0.031	0.028
MIR data for Haro 11				
Ion	F[d]	I/I(Hβ)[e]	I/I(Hβ)[f]	CLOUDY
10.51 μm [S IV]	4.395	0.122	0.365	0.224
12.81 μm [Ne II]	3.123	0.087	0.259	0.097
15.55 μm [Ne III]	9.814	0.273	0.814	0.466
18.71 μm [S III]	4.524	0.126	0.376	0.206

Notes. [(a)] Extinction-corrected fluxes. [(b)] B and C mean Haro 11B and Haro 11C, respectively. [(c)] Sum of the 3726 and 3728 [O II] lines. [(d)] Observed flux in units of 10^{-13} erg s^{-1} cm^{-2} (Wu et al. 2008). [(e)] Extinction-corrected flux ratios with C(Hβ) = 0.745. [(f)] Extinction-corrected flux ratios with C(Hβ) = 0.27.

The CLOUDY-predicted and extinction-corrected fluxes of bright emission lines in Haro 11B and Haro 11C are shown in Table 6. The overall agreement achieved implies that a H II region model including only the stellar ionising radiation of a single stellar population is able to account for the observed fluxes, in both the optical and NIR ranges. No additional excitation mechanism such as shocks from stellar winds and supernova remnants is needed. This conclusion also holds for the [Fe II] λ12570, 16436 Å emission lines (Table 6), which are often considered as shock indicators (e.g. Moorwood & Oliva 1988; Oliva et al. 1990, 2001).

We note that the photoionisation models for a single stellar population cannot reproduce the extinction-corrected fluxes in ESO 338-IG 004, because they are measured in the spectrum that includes two star-forming regions with different excitation properties. The superposition of two CLOUDY models should be used instead to fit the observations of ESO 338-IG 004.

To extend our study of Haro 11 into the MIR range, we used the *Spitzer* observations of Wu et al. (2008) obtained with an aperture, which is much larger than the one used in the X-shooter observations, and includes all of the bright H II regions

A, B, and C. Therefore, to compare the observed and CLOUDY-predicted emission-line fluxes in the MIR range (relative to Hβ) we should take into account aperture corrections. In particular, the extinction-corrected Hβ flux from the X-shooter observations cannot be used because it was obtained with a smaller aperture. We instead derive the Hβ extinction-corrected flux from the total Hα flux $F(\mathrm{H}\alpha) = 3.326 \times 10^{-12}$ erg s^{-1} cm^{-2} measured by Wu et al. (2008) after its correction for extinction. We do not know the average extinction coefficient $C(\mathrm{H}\beta)$ within an aperture used for the MIR observations by Wu et al. (2008). It is known from HST data (Adamo et al. 2010) that the reddening in Haro 11 varies in the range $E(B-V) = 0.0$ to 0.6 (corresponding to $C(\mathrm{H}\beta) = 0.0$ to 0.88), and to even higher values, in agreement with our extinction determinations for Haro 11B and Haro 11C. Therefore, to correct the Hβ flux for extinction within a large aperture, we consider two limiting cases by adopting the $C(\mathrm{H}\beta)$ values derived from both the Haro 11B spectrum (high extinction) and the Haro 11C spectrum (low extinction). It is also reasonable to assume that the averaged extinction in the area covered by the MIR observations is between these two limiting cases. In the third and fourth columns of Table 6, we show the MIR emission-line fluxes normalised to the extinction-corrected Hβ flux with $C(\mathrm{H}\beta) = 0.745$ (the case of Haro 11B) and $C(\mathrm{H}\beta) = 0.27$ (the case of Haro 11C), respectively. We also note that a correction of MIR emission lines for extinction is not needed. In the last column of Table 6 for MIR data, we show CLOUDY predictions with input parameters from Table 5. It is seen from Table 6 that the predicted relative MIR emission-line fluxes are between the two limiting cases of extinction-corrected fluxes with high and low extinctions, suggesting that with a more realistic intermediate extinction the agreement between models and observations would be much better. This implies that the MIR range, similar to the NIR range, does not resemble highly extincted emission-line regions that significantly contribute to the MIR line emission.

3.5. Evidence for luminous blue variable (LBV) stars in Haro 11

The Hα emission line in the spectrum of Haro 11C is asymmetric and has also a broad component. Östlin et al. (2001) also reported that the Hα line profiles of Haro 11 are broad, up to full widths at half maximum (FWHM) of 270 km s^{-1}, and have a non-Gaussian shape. They suggested that two or more non-virialised ionised gas components may be present in the galaxy. The extinction-corrected relative Hα flux $I(\mathrm{H}\alpha)/I(\mathrm{H}\beta) = 3.82$ in Haro 11C, obtained with $C(\mathrm{H}\beta) = 0.27$, deviates significantly from the theoretical recombination value 2.86 (Hummer & Storey (1987) for the electron temperature 10 000 K and the electron number density $N_e = 100$ cm^{-3} when the observed Hα flux $F(\mathrm{H}\alpha) = 3.350 \times 10^{-14}$ erg s^{-1} cm^{-2} is adopted. This high Hα flux may be due to substantial emission from either supernovae of type II or circumstellar envelopes of stars. Because of its anomalous behavior this line was excluded in Sect. 3.1 from the calculation of the extinction coefficient. The decomposition of the Hα emission line of Haro 11C into three Gaussian emission components and one Gaussian absorption component is shown in Fig. 5. Two of the Gaussian emission components (the narrowest and the broadest) marked by blue dotted lines are likely linked to the nebular emission, implying that there is low- and high-velocity ionised gas in the H II region. These two components are sufficient to reproduce the shape of the strongest forbidden line [O III] λ5007, strengthening the evidence for a nebular origin of these components. However, the Hα profile is more complex, and two additional components (emission and absorption) are needed. The green dotted line is the composition of the third emission and absorption components and represents a P Cyg profile. The observed Hα profile (black solid line) is nicely fit by the summed profile, consisting of two nebular components and the P Cyg profile (red dashed line). The flux $F(\mathrm{H}\alpha) = 2.281 \times 10^{-14}$ erg s^{-1} cm^{-2} of the Hα line after subtraction of the P Cyg profile corresponds to the recombination ratio $I(\mathrm{H}\alpha)/I(\mathrm{H}\beta) = 2.86$ (Table 1) after the correction for extinction with $C(\mathrm{H}\beta) = 0.27$ is applied. Thus, the inclusion of the stellar component of Hα emission is required to fit the observations, implying that either LBV star(s) or supernovae are present. The Hα emission line is therefore the most affected by the presence of a stellar wind. The observed Balmer decrement of the broad emission lines in LBVs and SNe is often much larger than that for the narrow lines, reflecting the high density and possibly high extinction in the circumstellar envelopes where the broad lines originate. In particular, this is true for the LBV in PHL 293B and results in a very strong Hα emission line compared to the Hβ line (Izotov & Thuan 2009; Izotov et al. 2011b). On the other hand, the small FWHM of ~180 km s^{-1} of the P Cyg component precludes the supernovae scenario. We note that, in principle, in ESO 338-IG 004 some additional contribution from LBV stars or shocks to the Hα emission can also be present. Therefore, $C(\mathrm{H}\beta)$ was derived excluding Hα, hence $I(\mathrm{H}\alpha)/I(\mathrm{H}\beta) = 2.94$ (Table 1) is slightly higher than the recombination ratio.

The extinction-corrected luminosity of the Hα P Cyg component in Haro 11C is very high, $L(\mathrm{P\ Cyg}) = 1.32 \times 10^{40}$ erg s^{-1}, exceeding by a factor of ~10–100 the Hα luminosities of LBV stars in the low-metallicity emission-line galaxies NGC 2366 (Drissen et al. 1997, 2001), PHL 293B, and DDO 68 (Izotov et al. 2007; Izotov & Thuan 2009; Izotov et al. 2011b).

Moreover, sixteen permitted Fe II emission lines are observed in the spectra of Haro 11B and Haro 11C (see Figs. 4, 1, 2, 3 and Table 1), which reflects their circumstellar origin in the dense stellar wind. No such lines are present in low-density nebular gas. The Orion Nebula serves as a template for the investigation of different excitation mechanisms of emission lines observed in a gaseous nebulae. It is one of the most well-studied of nearby Galactic H II regions with an extensive list of identifications of various lines, including the very weak ones (e.g. Peimbert & Torres-Peimbert 1977; Osterbrock et al. 1992). There are high-resolution spectroscopic observations of the Orion nebula with high signal-to-noise ratios. Nevertheless, the Fe II lines observed in the VLT/X-shooter spectra of Haro 11B and C are not present in the spectra of the Orion nebula obtained by Baldwin et al. (2000), Esteban et al. (2004), and Mesa-Delgado et al. (2009).

On the other hand, the permitted Fe II emission lines are common in spectra of LBV stars undergoing giant eruption events during the late evolutionary stages of the most massive stars. One of the most well-known LBVs is the binary system η Carina (η Car), which undergoes periodical outbursts (e.g. Massey 2003; Smith et al. 2004; Damineli et al. 2008b; Clark et al. 2005; Damineli et al. 2008a; Soker & Kashi 2012). The bright emission lines of H, He, and the permitted Fe II and forbidden [Fe II] lines are observed in LBVs that also display P Cyg profiles during eruption events. Most of the emission lines of different species (Mg I, [Fe II], Si II, [Ni II], [Cr II], N I, and [C I]) (Table 1) are observed in nebulae as well as in emission-line stars like LBVs, supergiants with H and He emission, and Of/WN9 stars. We also note that all Fe II emission lines seen in the spectra of Haro 11B and Haro 11C are detected only in the high-resolution spectra of η Car by e.g. Hamann et al. (1994) and Wallerstein et al. (2001). For the line identification, we use the data for η Car

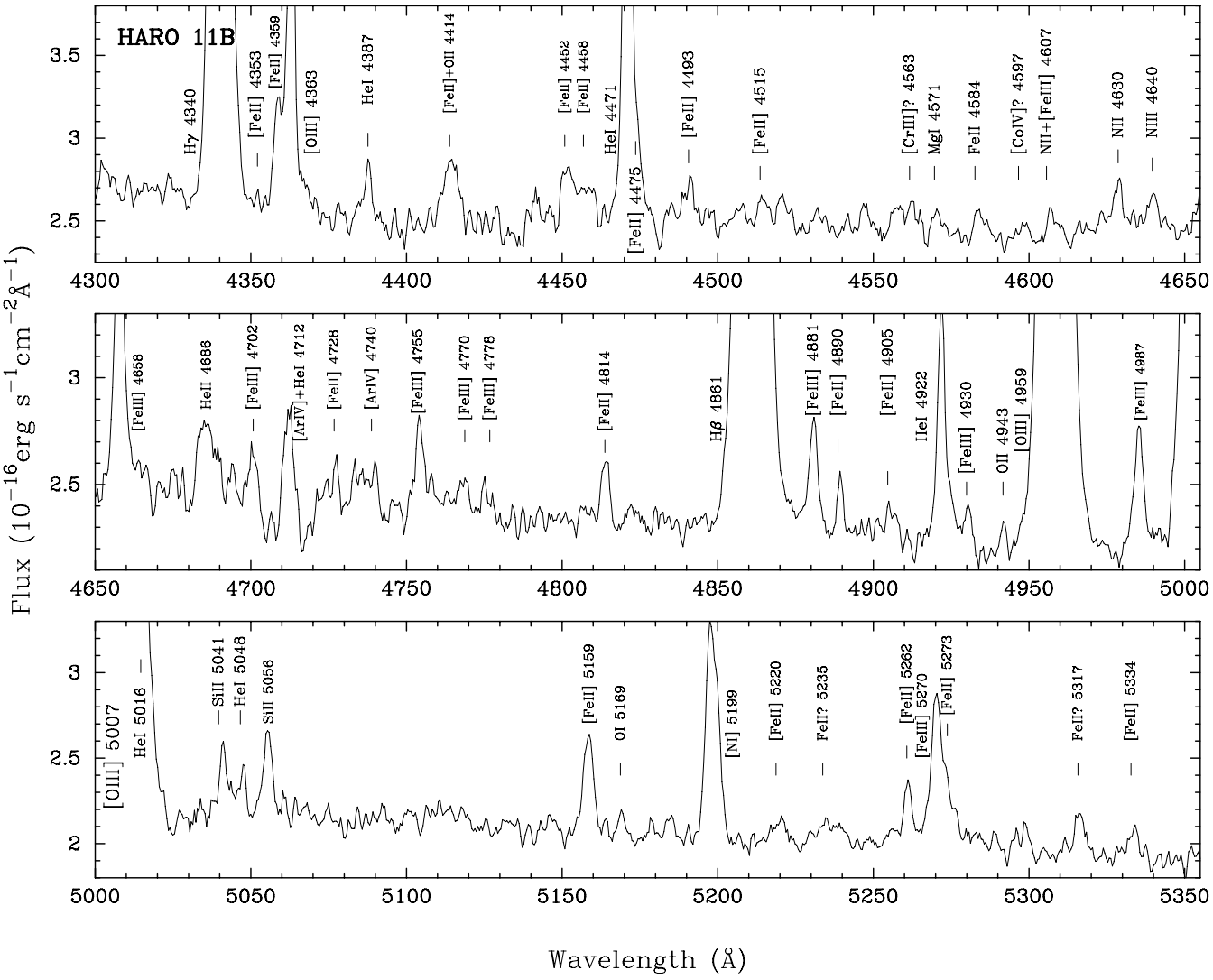

Fig. 4. Close-up part of the Haro 11B optical spectrum shown in Fig. 1.

of Wallerstein et al. (2001) in a wide wavelength range ~λ3100–9000 Å (with several gaps due to observational program reasons or telluric absorption) and data of Hamann et al. (1994) in the wavelength range ~λ6450–24 500 Å. These two sets of data cover the whole wavelength range of the VLT/X-shooter observations excluding gaps. Additionally, for some line identifications we used the data of Gaviola (1953), Johansson (1977), and Allen et al. (1985).

We find that LBV is probably also present in Haro 11B. This is indicated by the Fe II and [Fe II] emission lines in its spectrum (Fig. 4, Table 1). It is also possible that broad Hα emission is also present, but masked by very strong nebular Hα and [N II] λ6548, 6583 Å emission lines. On the other hand, no permitted Fe II emission lines were detected in the spectrum of ESO 338-IG 004 (see Table 1).

Thus, we have three pieces of evidence supporting the idea that a LBV star is present in Haro 11C. These are that a) a P Cyg profile is needed to reproduce the observed Hα profile, b) the only possible way to adjust the observed Balmer decrement to the theoretical one is the subtraction of the P Cyg component from the Hα emission line, and c) the presence of numerous Fe II emission lines, which is a common feature of the LBV star spectrum.

Smith et al. (2011) collected data for a number of extragalactic optical transients or "supernova impostors" related to giant eruptions of LBVs and illustrated their remarkably wide diversity in terms of their peak absolute magnitude, duration, progenitor stars, outburst spectra, and other observable properties. In particular, the peak absolute magnitude varies from –10 mag to –16 mag and increases during eruption by more than 2–4 mag for LBV stars of the Milky Way (η Car, P Cyg), V1 in NGC 2366, HD 5980 in the SMC, and others. There is not much information in the literature about the range of LBV Hα luminosities, but it is likely that they have a large range, which is similar to the absolute magnitudes. Therefore, it is difficult to quantitatively estimate the number of LBV stars in Haro 11C.

3.6. Spectral energy distributions, stellar masses and a red continuum excess

We derive the stellar masses of three H II regions (see Table 3) by fitting their spectra to a superposition of SEDs of single stellar populations with different ages following the prescriptions of Guseva et al. (2006, 2007) and Izotov et al. (2011a). This technique also allows us to check whether a red continuum excess is present in the spectra of Haro 11B and Haro 11C. We note, that for star-forming galaxies with $EW(H\beta) \geq 100$ Å the ionised

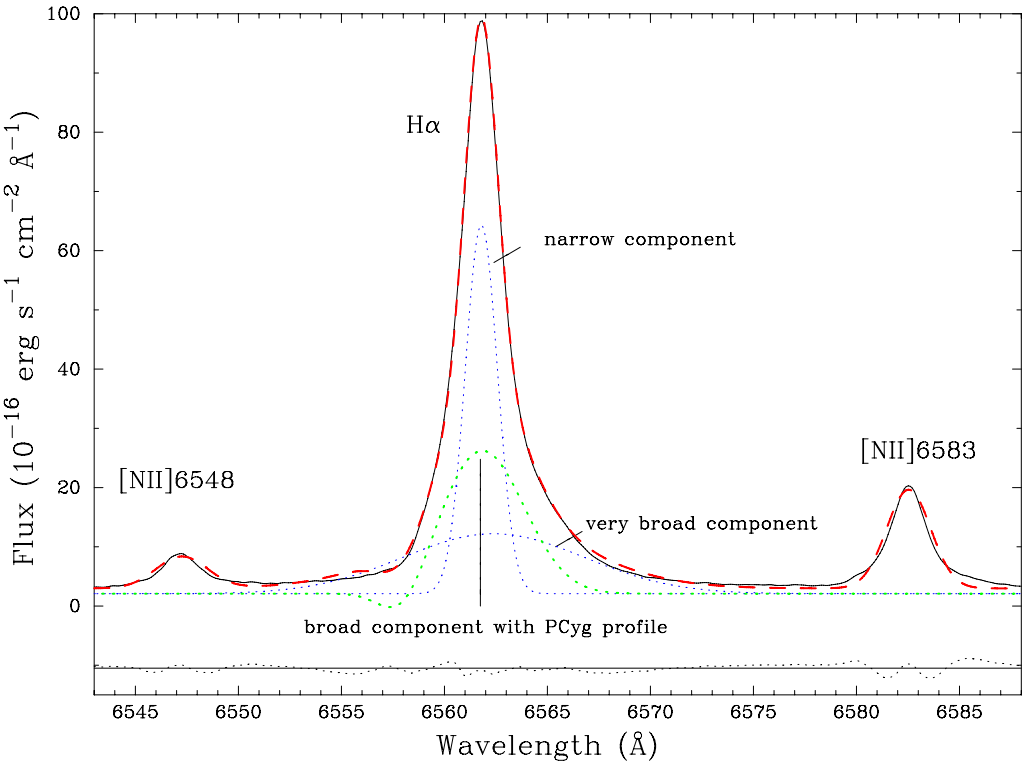

Fig. 5. Decomposition of the Hα emission-line profile in the Haro 11C spectrum. Two Gaussian components (blue dotted lines) are likely related to nebular emission, a P Cyg profile (green dotted line) is a spectral feature of an LBV star. The residual is shown by the black dotted line. For a better view this is shifted below the zero value. Observational data are shown by the black solid line and the modelled profile, which includes all components, is displayed by the red dashed line.

gas continuum emission contributes appreciably to the total continuum emission. Neglecting it can lead to an overestimation of galactic stellar masses by a factor of a few (Izotov et al. 2011a). We include the ionised gas emission in the fit of the spectra of all three objects, despite the equivalent width of the Hβ emission line being large (EW(Hβ) = 155 Å) only in the Haro 11B spectrum, while EW(Hβ) < 100 Å in the spectra of Haro 11C and ESO 338-IG 004 (Table 1).

As each SED is the sum of both stellar and ionised gas emission, its shape depends on the relative contributions of these two components. In active star-forming regions, the contribution of the ionised gas emission can be very large. However, the equivalent widths of the Hβ emission line never reach the theoretical values for pure gaseous emission of ~900–1100 Å, implying that there is a non-zero contribution of stellar emission in all objects. To take into account gaseous emission, we use the observed emission-line fluxes and equivalent widths. The contribution of the gaseous emission is scaled to the stellar emission using the ratio of the observed equivalent width of the Hβ emission line to the equivalent width of Hβ expected for pure gaseous emission. The continuous gaseous emission is taken from Aller (1984) and includes hydrogen and helium free-bound, free-free and two-photon emission. In our models, this emission is always calculated using the electron temperature $T_e(H^+)$ of the H^+ zone and with the He/H abundance ratio derived from the H II region spectrum.

To calculate the contribution of stellar emission to the SEDs, we adopt a grid of the Padua stellar evolution models of Girardi et al. (2000)[2] with a heavy element mass fraction Z = 0.008 for Haro 11B and Z = 0.004 for Haro 11C and ESO 338-IG 004. Using these data, we calculate with the package PEGASE.2 (Fioc & Rocca-Volmerange 1997) a grid of stellar instantaneous burst SEDs for a range of ages from 0.5 Myr to 15 Gyr. We adopt a stellar initial mass function with a Salpeter slope, an upper mass limit of 100 $M_\odot$, and a lower mass limit of 0.1 $M_\odot$. The SED for any star formation history (SFH) can then be obtained by integrating the instantaneous burst SEDs over time with a specified time-varying SFR. We approximate the SFH by a combination of a recent short burst to account for the young stellar population, and continuous star formation to describe the properties of the older stars.

Finally, the contribution of the nebular continuum and emission lines were taken into account. Each fit was performed over the whole observed spectral range ~$\lambda\lambda$3000–24 000 Å. We performed 5×10^5 Monte Carlo models by varying simultaneously the age of young stellar population t(young), the age of the oldest stars t(old), the mass ratio of old-to-young stellar populations $b = M(\text{old})/M(\text{young})$, the electron temperature $T_e(H^+)$ in the H^+ zone, and the extinction coefficients for gas and for stars, $C(H\beta)_{gas}$ and $C(H\beta)_{stars}$, respectively.

The best-fit model SED is found from χ^2 minimisation of the deviation between the modelled and the observed continuum in ten ranges of the whole spectrum free of emission lines.

In Fig. 6, we show the best-fit model SED fits to the redshift- and extinction-corrected spectra of Haro 11B, C, and ESO 338-IG 004. The contributions from the stellar and ionised gas components are shown by green and blue lines, respectively. The sum of both stellar and ionised gas emission is shown by a red line. It is seen that the contribution of gaseous emission is essential only for Haro 11B because of the high EW(Hβ). For an other two objects, this contribution is small, especially for Haro 11C with EW(Hβ) = 16 Å.

[2] http://pleiadi.pd.astro.it

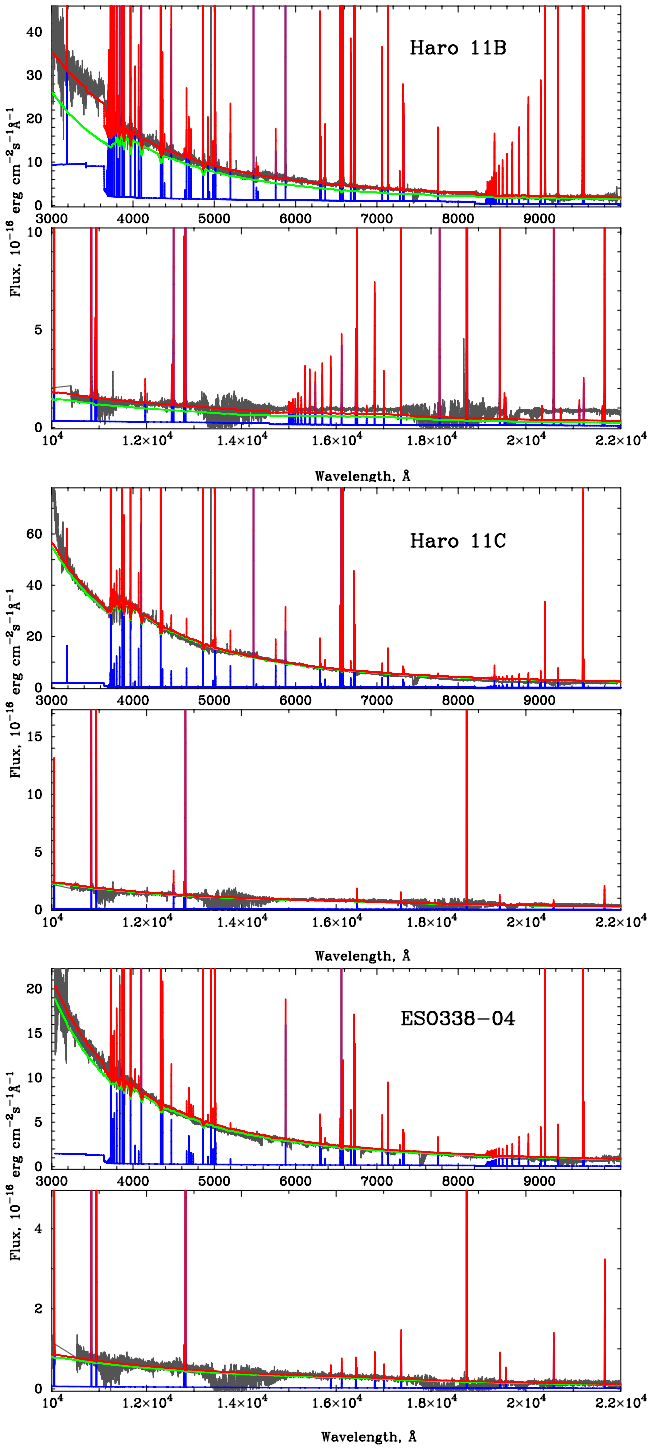

Fig. 6. Best-fit model SED fits to the redshift- and extinction-corrected observed spectra of Haro 11B, Haro 11C, and ESO 338-IG 004. The contributions from the stellar and ionised gas components are shown by the green and blue lines, respectively. The sum of stellar and ionised gas emission is shown by the red line.

Adamo et al. (2010) found using HST photometry data for Haro 11, that a strong red excess is present in spectra of Haro 11B and Haro 11C at wavelengths >8000 Å with respect to the synthetic evolutionary models. They show that despite the tighter model fit to the Haro 11B spectrum achieved (χ^2 for Haro 11B is smaller than that for Haro 11C), the red excess in Haro 11B is larger. Figure 6 shows that all observed spectra in the whole range of wavelengths ~$\lambda\lambda$3000–24 000 Å are fitted quite well by the model SEDs, except for the spectrum of Haro 11B where the flux excess at wavelengths >1.6 μm is clearly present. Thus, Adamo et al. (2010) found red excesses in the B and C knots but in the present paper we find one only for the B knot. This disagreement can be partially associated with the different sizes of the extracted regions (we adopted extraction apertures of ~1″ × 4″ for Haro 11B and C, while Adamo et al. (2010) adopted much smaller apertures). However, we note that the majority of the light in the B and C knots within the large adopted spectroscopic apertures comes from the brightest compact clusters within the slit, implying that we measure similar continuum flux densities to those in the photometric study of Adamo et al. (2010).

Table 7. Equivalent widths of the stellar absorption CO band (λ = 2.3 μm) in Haro 11.

	Starburst-99[a,b]			
	Inst.[c]		Cont.[d]	
Observations	Z = 0.004	Z = 0.008	Z = 0.004	Z = 0.008
Haro 11B 8 Å	8–11 Å	13–15 Å	2–8 Å	8–10 Å
Haro 11C 9 Å				

Notes. [a] Values for the time of 8–10 Myr after the onset of star formation (Leitherer et al. 1999). [b] Z is heavy element mass fraction. [c] Instantaneous burst model. [d] Continuous star formation.

What is the nature of this excess? As mentioned above the observed fluxes of the Balmer, Paschen, and Brackett hydrogen lines after correction for extinction with a single value C(Hβ) (see Table 1) agree well with the theoretical recombination values of Hummer & Storey (1987) for all studied star-forming regions, i.e. Haro 11B, Haro 11C, and ESO 338-IG 004. The same result was obtained from CLOUDY modelling (Table 6). This implies that the NIR excess is not due to highly obscured hot stars ionising the interstellar medium, which would require that the continuum excess be followed by an excess of the NIR emission lines, a result we do not find. Evidently, only the non-ionising cool stars, including a large population of luminous red supergiant stars (RSGs), can contribute to the NIR continuum excess.

This conclusion is supported by the detection of the strongest stellar absorption CO band at ~2.3 μm in the spectra of Haro 11B and Haro 11C. This spectral feature is a signature of red giant and red supergiant stars. The equivalent width of the CO band depends on stellar temperature and luminosity and decreases with both increasing stellar temperature and decreasing stellar luminosity. We measure equivalent widths EW(CO 2.3 μm) of 8 Å and 9 Å in Haro 11B and Haro 11C, respectively. In Table 7, we compare the observed values with the Starburst-99 stellar population synthesis models (Leitherer et al. 1999) and conclude that the stellar population of an older burst with an age of ~10 Myr including red supergiant stars can be responsible for the observed red excess and CO absorption at ~2.3 μm. This older non-ionising stellar population is probably more obscured by the dust and therefore does not contribute to the optical light. However, we are unable to infer whether this is true from the hydrogen-line decrement because the older population does not produce emission in hydrogen lines.

We derive the instantaneous SFR(Hα), using the extinction-corrected luminosity L(Hα) of the Hα emission line and the frequently used relation by Kennicutt (1998), which, however, is obtained for longer-duration star formation in disc galax-

ies and may not be valid for knots B and C where stars were formed almost instantaneously. We obtain SFR = 3.5, 0.22, and 0.11 $M_\odot$ yr^{-1} in Haro 11B, Haro 11C, and ESO 338-IG 004, respectively, for the regions within the apertures used for the spectroscopic observations (see sect. 2). To achieve this result, we adopt the distances of 82.4 Mpc and 38.4 Mpc for Haro 11 and ESO 338-IG 004, respectively, which are taken from the NED. The star formation rates of luminous compact emission-line galaxies (LCGs) derived by Izotov et al. (2011a) are in the range 0.7–60 $M_\odot$ yr^{-1} with an average value of ∼4 $M_\odot$ yr^{-1}. Thus, Haro 11 is among the galaxies with significant star-formation activity in its H II region B. The specific star formation rates (SSFR) are then defined as SSFR(Hα) = SFR(Hα)/M_* and are equal to 2.8×10^{-8} yr^{-1}, 1.1×10^{-9} yr^{-1}, and 2.0×10^{-9} yr^{-1} for Haro 11B, Haro 11C, and ESO 338-IG 004, respectively. In addition, the SSFR for Haro 11B is high and similar to those found in LCGs by Izotov et al. (2011a) and in high-redshift galaxies, while the SSFRs for Haro 11C and ESO 338-IG 004 are lower by a factor of ∼10.

4. Conclusions

We have studied the spectra of the blue compact galaxies Haro 11 and ESO 338-IG 004 obtained by performing VLT/X-shooter spectroscopic observations in the wavelength range ∼$\lambda\lambda$3000–24 000 Å. We have arrived at the following conclusions:

1. We derived oxygen abundances of 12 + log O/H = 8.33 ± 0.01 and 8.10 ± 0.04 in the two H II regions Haro 11B and Haro 11C, respectively, which are appreciably higher than the previous determination of Bergvall & Östlin (2002) (12 + log O/H = 7.9). Our oxygen abundance 12 + log O/H = 7.89 ± 0.01 for ESO 338-IG 004 is slightly lower than the previous determinations, which are in the range 7.92–8.08 (Masegosa et al. 1994; Bergvall 1985; Raimann et al. 2000; Bergvall & Östlin 2002; Guseva et al. 2011a).
2. We used X-shooter data together with *Spitzer* observations in the mid-infrared range to test for hidden star formation. The observed fluxes of hydrogen lines correspond to the theoretical recombination values after correction for extinction with a single value of C(Hβ) applied to a wide wavelength range from near-UV to NIR and MIR. Thus, we confirm our previous findings obtained for several low-metallicity emission-line galaxies (Mrk 59, II Zw 40, Mrk 71, Mrk 996, SBS 0335–052E, PHL 293B, and GRB HG 031203) that the extinction coefficient C(Hβ) is not systematically higher in the NIR wavelength range than the optical one and that no hidden star formation contributes appreciably to the NIR line emission but not the optical line emission.
3. All observed spectra are fitted quite well across the entire wavelength range covered by model SEDs, except for the continuum flux excess at wavelengths >1.6 μm for Haro 11B. An anomalously large population of luminous red supergiant stars (RSGs) in Haro 11B is probably responsible for the observed flux excess relative to the model SED in the NIR range.
4. Thirteen ro-vibrational H_2 emission lines are detected in the NIR spectrum of Haro 11B. From the observed flux ratios of the H_2 lines, we conclude that fluorescence is the main excitation mechanism of ro-vibrational H_2 lines. This confirms the previous finding for BCGs with high-excitation H II regions.
5. The agreement between the CLOUDY-predicted and extinction-corrected emission-line fluxes implies that a H II region model including only stellar photoionisation as an ionising source is able to account for the observed fluxes in the optical, NIR, and MIR ranges. No additional excitation mechanism such as shocks from stellar winds and supernova remnants is needed.
6. We find evidence of an LBV star in Haro 11C: a) a P Cyg profile is needed to reproduce the asymmetric Hα emission line; b) the same P Cyg emission is needed to explain a strong Hα emission excess above the recombination value; c) numerous permitted singly ionised iron emission lines are detected in the spectrum of Haro 11C. These lines are common in the spectra of LBV stars. The high luminosity of the P Cyg Hα line L(P Cyg) = 1.3×10^{40} erg s^{-1} exceeds by a factor of 10–100 the LBV luminosities in some low-metallicity emission-line galaxies. Similarly, the numerous Fe II and [Fe II] emission lines in the spectrum of Haro 11B indicates that LBV is also present in this knot. We find no evidence of LBV in ESO 338-IG 004.

Acknowledgements. N.G.G., Y.I.I., and K.J.F. are grateful to the staff of the Max Planck Institute for Radioastronomy for their warm hospitality. This research has made use of the NASA/IPAC Extragalactic Database (NED), which is operated by the Jet Propulsion Laboratory, California Institute of Technology, under contract with the National Aeronautics and Space Administration.

References

Adamo, A., Östlin, G., Zackrisson, E., et al. 2010, MNRAS, 407, 870
Allen, D. A., Jones, T. J., & Hyland, A. R. 1985, ApJ, 291, 280
Aller, L. H. 1984, Physics of Thermal Gaseous Nebulae (Dordrecht: Reidel)
Asplund, M., Grevesse, N., Sauval, A. J., & Scott, P. 2009, ARA&A, 47, 481
Baldwin, J. A., Verner, E. M., Verner, G. J., et al. 2000, ApJS, 129, 229
Bergvall, N. 1985, A&A, 146, 269
Bergvall, N., & Östlin, G. 2002, A&A, 390, 891
Bergvall, N., Masegosa, J., Östlin, G., & Cernicharo, J. 2000, A&A, 359, 41
Black, J. H., & van Dishoeck, E. F. 1987, ApJ, 322, 412
Bohlin, R. C. 1996, AJ, 111, 1743
Cardamone, C., et al. 2009, MNRAS, 399, 1199
Cardelli, J. A., Clayton, G. C., & Mathis, J. S. 1989, ApJ, 345, 245
Clark, J. S., Larionov, V. M., & Arkharov, A. 2005, A&A, 435, 239
Colina, L., & Bohlin, R. C. 1994, AJ, 108, 1931
Cresci, G., Vanzi, L., Sauvage, M., Santangelo, G., & van der Werf, P. 2010, A&A, 520, 82
Damineli, A., Hillier, D. J., Corcoran, M. F., et al. 2008a, MNRAS, 384, 1649
Damineli, A., Hillier, D. J., Corcoran, M. F. et al. 2008b, MNRAS, 386, 2330
Drissen, L., Roy, J.-R., & Robert, C. 1997, ApJ, 474, L35
Drissen, L., Crowther, P. A., Smith, L. J., et al. 2001, ApJ, 546, 484
Esteban, C., Peimbert, M., García-Rojas, J., et al. 2004, MNRAS, 355, 229
Ferland, G. J., Korista, K. T., Verner, D. A., et al. 1998, PASP, 110, 761
Fioc, M., & Rocca-Volmerange, B. 1997, A&A, 326, 950
Garnett, D. R., Skillman, E. D., Dufour, R. J., et al. 1995, ApJ, 443, 64
Gaviola, E. 1953, ApJ, 118, 234
Girardi, L., Bressan, A., Bertelli, G., & Chiosi, C. 2000, A&AS, 141, 371
Guseva, N. G., Izotov, Y. I., & Thuan, T. X. 2006, ApJ, 644, 890
Guseva, N. G., Izotov, Y. I., Papaderos, P., & Fricke, K. J. 2007, A&A, 464, 885
Guseva, N. G., Izotov, Y. I., Stasinska, G., et al. 2011a, A&A, 529, 149
Guseva, N. G., Izotov, Y. I., Fricke, K. J., & Henkel, C. 2011b, A&A, 534, 84
Hamann, F., DePoy, D. L., Johansson, S., & Elias, J. 1994, ApJ, 422, 626
Hayes, M., Östlin, G., Atek, H., et al. 2007, MNRAS, 382, 1465
Hirashita, H., & Hunt, L. K. 2004, A&A, 421, 555
Hummer, D. G., & Storey, P. J. 1987, MNRAS, 224, 801
Izotov, Y. I., & Thuan, T. X. 2004, ApJ, 602, 200
Izotov, Y. I., & Thuan, T. X. 2009, ApJ, 690, 1797
Izotov, Y. I., & Thuan, T. X. 2011, ApJ, 734, 82
Izotov, Y. I., Thuan, T. X., & Lipovetsky, V. A. 1994, ApJ, 435, 647
Izotov, Y. I., Stasińska, G., Guseva, N. G., & Thuan T. X. 2004, A&A, 415, 87
Izotov, Y. I., Stasińska, G., Meynet, G., Guseva, N. G., & Thuan T. X. 2006, A&A, 448, 955
Izotov, Y. I., Thuan, T. X., & Guseva, N. G. 2007, ApJ, 671, 1297
Izotov, Y. I., Thuan, T. X., & Wilson, J. C. 2009, ApJ, 703, 1984

Izotov, Y. I., Guseva, N. G., & Thuan, T. X. 2011a, ApJ, 728, 161
Izotov, Y. I., Guseva, N. G., Fricke, K. J., & Henkel, C. 2011b, A&A, 533, 25
Johansson, S. 1977, MNRAS, 178, 17
Kennicutt, R. C. Jr. 1998, ARA&A, 36, 189
Kunth, D., Leitherer, C., Mas-Hesse, J. M., Östlin, G., & Petrosian, A. 2003, ApJ, 597, 263
Leitherer, C., Schaerer, D., Goldader, J. D., et al. 1999, ApJS, 123, 3
Masegosa, J., Moles, M., & Campas-Aguilar, A. 1994, ApJ, 420, 576
Massey, P. 2003, ARA&A, 41, 15
Mesa-Delgado, A., Esteban, C., García-Rojas, J., et al. 2009, MNRAS, 395, 855
Meurer, G. R., Heckman, T. M., Leitherer, C., et al. 1995, AJ, 110, 2665
Micheva, G., Zackrisson, E., Östlin, G., Bergvall, N., & Pursimo, T. 2010, MNRAS, 405, 1203
Moorwood, A. F. M., & Oliva, E. 1988, A&A, 203, 278
Oke, J. B. 1990, AJ, 99, 1621
Oliva, E., Moorwood, A. F. M., & Danziger, I. J. 1990, A&A, 240, 453
Oliva, E., Marconi, A., Maiolino, R., et al. 2001, A&A, 369, L5
Osterbrock, D. E., Tran, H. D., & Veilleux, S. 1992, ApJ, 389, 305
Östlin, G., Bergvall, N., & Roñnback, J. 1998, A&A, 335, 85
Östlin, G., Amram, P., Bergvall, N., et al. 2001, A&A, 374, 800
Östlin, G., Cumming, R. J., & Bergvall, N. 2007, A&A, 461, 471
Östlin, G., Hayes, M., Kunth, D., et al. 2009, AJ, 138, 923
Overzier, R. A., Heckman, T. M., & Kauffmann, G. 2008, ApJ, 677, 37
Peimbert, M., & Torres-Peimbert, S. 1977, MNRAS, 179, 217
Pettini, M., Shapley, A. E., Steidel, C. C., et al. 2001, ApJ, 554, 981
Raimann, D., Storchi-Bergmann, T., Bica, E., Melnick J., & Schmitt, H. 2000, MNRAS, 316, 559
Smith, N., Morse, J. A., Gull, T. R., et al. 2004, ApJ, 605, 405
Smith, N., Li, W., Silverman, J. M., Ganeshalingam, M., & Filippenko, A. V. 2011, MNRAS, 415, 773
Soker, N., & Kashi, A. 2012, New Astron., in press [arXiv:1111.1454v1]
Terlevich, R., Melnick, J., Masegosa, J., Moles, M., & Copetti, M. V. F. 1991, A&AS, 91, 285
Vader, J. P., Frogel, J. A., Terndrup, D. M., & Heisler, C. A. 1993, AJ, 106, 1743
Vanzi, L., Hunt, L. K., Thuan, T. X., & Izotov, Y. I. 2000, A&A, 363, 493
Vanzi, L., Hunt, L. K., & Thuan, T. X. 2002, A&A, 390, 481
Vanzi, L., Cresci, G., Telles, E., & Melnick, J. 2008, A&A, 486, 393
Wallerstein, G., Gilroy, K. K., Zethson, T., Johansson, S., & Hamann, F. 2001, PASP, 113, 1210
Wu, Y., Bernard-Salas, J., Charmandaris, V., et al., ApJ, 2008, 673, 193

Pages 12 to 19 are available in the electronic edition of the journal at http://www.aanda.org

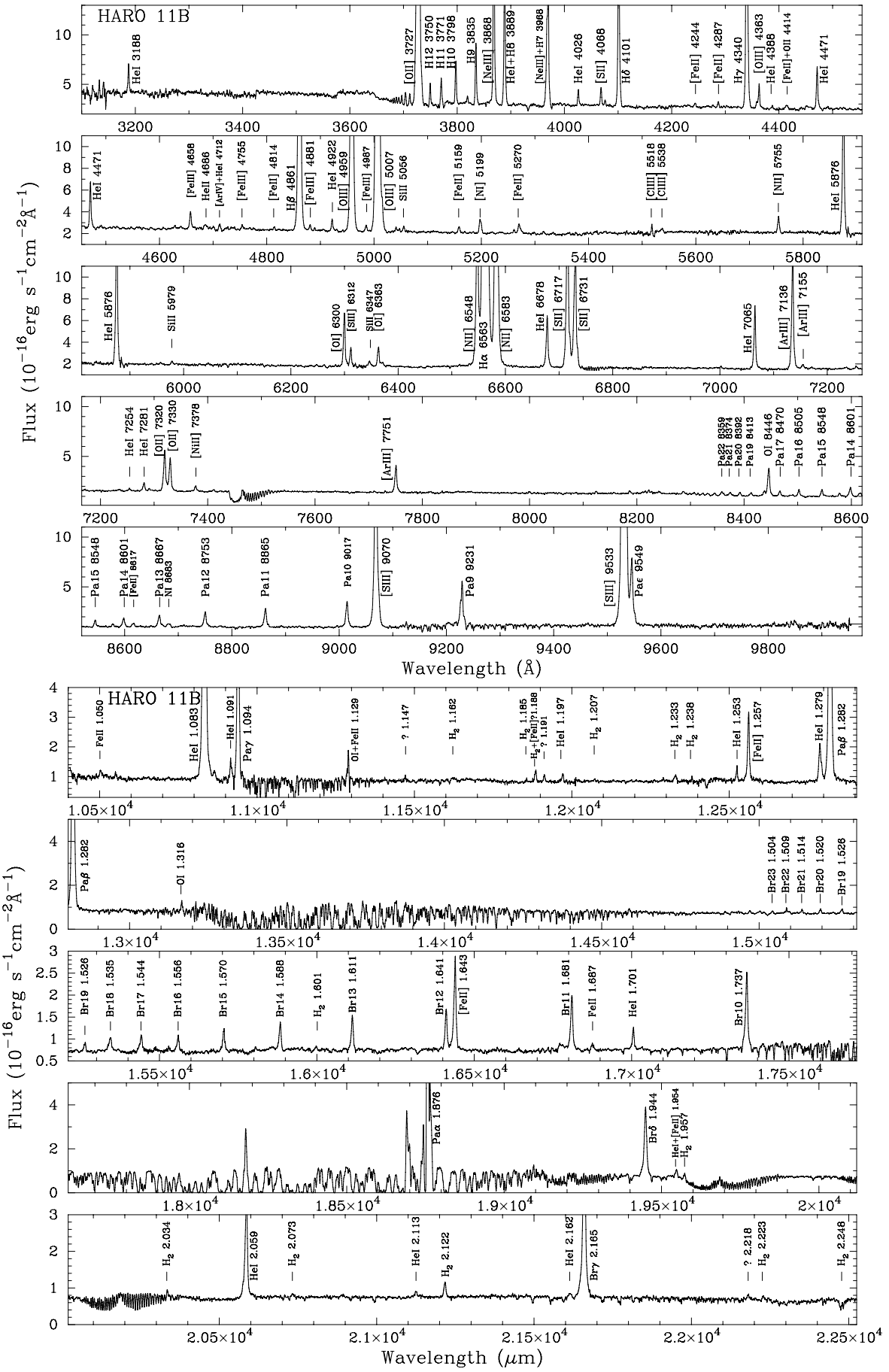

Fig. 1. Redshift-corrected VLT/X-shooter spectrum of Haro 11B with identifications of strong lines. Dubious identifications are marked with "?".

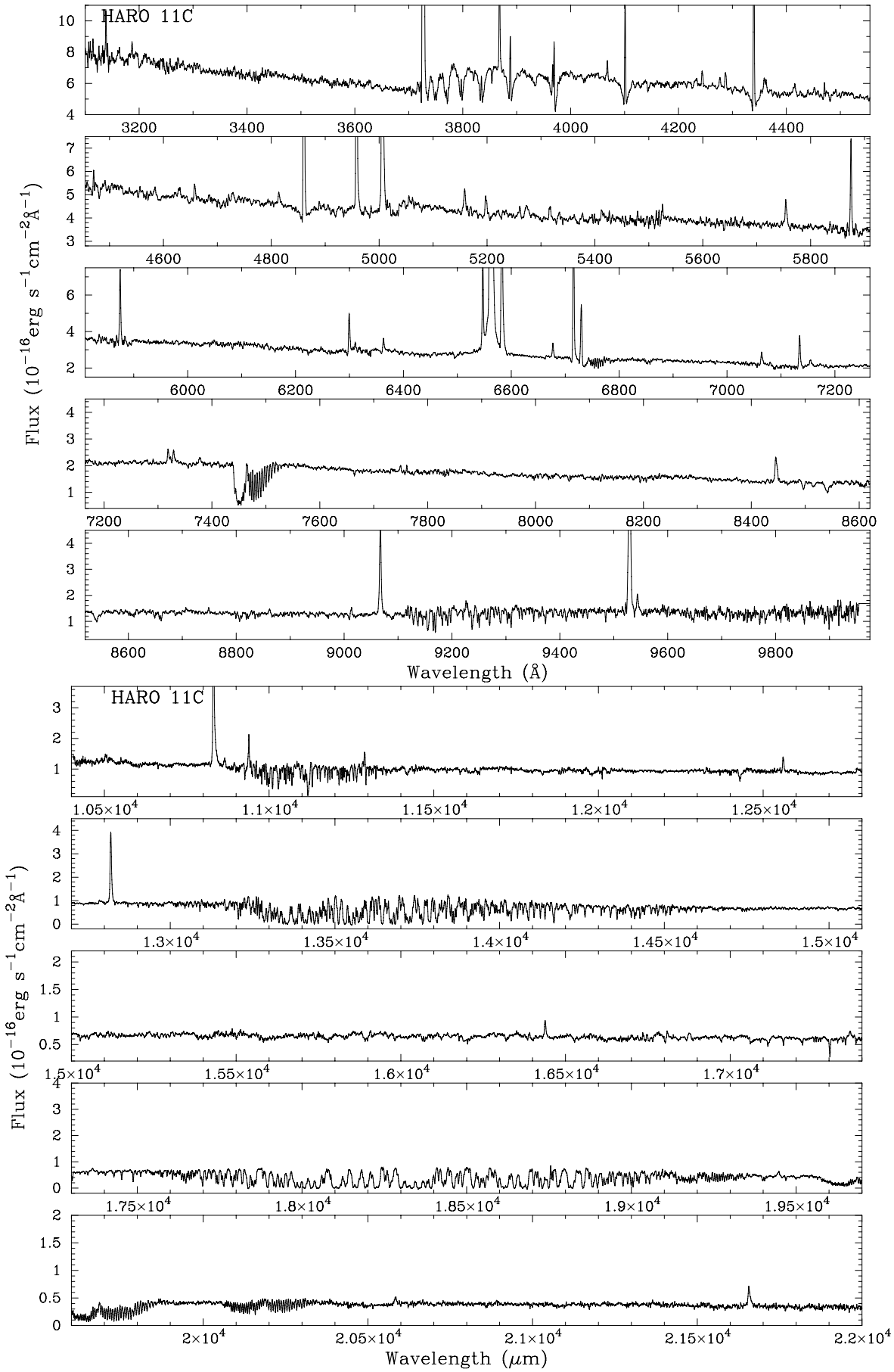

Fig. 2. Same as Fig. 1 but for Haro 11C.

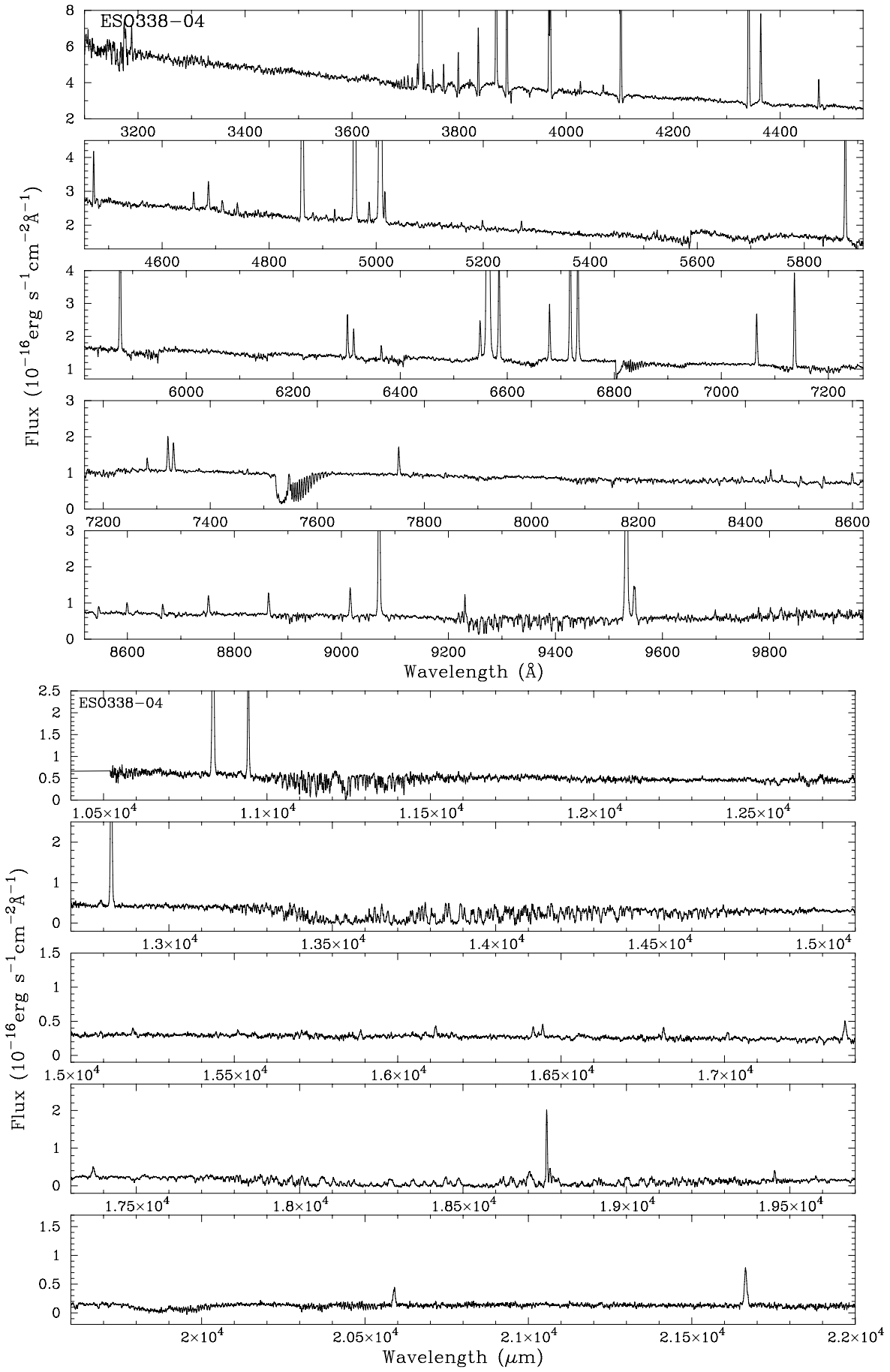

Fig. 3. Same as Fig. 1 but for ESO 338-IG 004.

Table 1. Emission line intensities.

	Galaxy						
	Haro 11B		Haro 11C		ESO 338-IG 004		theory
Ion	$F(\lambda)/F(\mathrm{H}\beta)^a$	$I(\lambda)/I(\mathrm{H}\beta)^b$	$F(\lambda)/F(\mathrm{H}\beta)^a$	$I(\lambda)/I(\mathrm{H}\beta)^b$	$F(\lambda)/F(\mathrm{H}\beta)^a$	$I(\lambda)/I(\mathrm{H}\beta)^b$	Case B^c
			a) Near-UV and optical range				
3188 He I	2.14 ± 0.07	4.92 ± 0.16	3.01 ± 0.32	3.99 ± 0.43	...	...	...
3322 [Fe III]?	0.21 ± 0.04	0.45 ± 0.10	...	...	...	...	...
3614 He I	0.19 ± 0.03	0.34 ± 0.05	...	...	...	...	...
3634 He I	0.15 ± 0.03	0.26 ± 0.05	...	...	...	...	...
3671 H24	0.16 ± 0.04	0.31 ± 0.08	...	...	0.19 ± 0.04	0.24 ± 0.05	0.39
3676 H22	0.24 ± 0.04	0.40 ± 0.07	...	...	0.42 ± 0.05	0.53 ± 0.06	0.50
3679 H21	0.25 ± 0.03	0.43 ± 0.05	...	...	0.34 ± 0.04	0.43 ± 0.06	0.57
3683 H20	0.30 ± 0.02	0.51 ± 0.03	...	...	...	...	0.66
3687 H19	0.34 ± 0.02	0.59 ± 0.03	...	...	...	...	0.77
3692 H18	0.49 ± 0.02	0.85 ± 0.03	...	...	...	...	0.91
3697 H17	0.61 ± 0.02	1.05 ± 0.04	...	...	...	...	1.08
3704 H16	1.06 ± 0.03	1.82 ± 0.05	...	...	...	...	1.29
3712 H15	0.97 ± 0.03	1.66 ± 0.05	...	...	...	...	1.57
3722 H14	1.82 ± 0.04	3.09 ± 0.07	1.41 ± 0.14	1.67 ± 0.17	...	...	1.93
3726 [O II]	63.69 ± 0.91	107.80 ± 1.68	85.01 ± 1.25	100.74 ± 1.64	46.53 ± 0.70	57.82 ± 0.94	...
3728 [O II]	65.57 ± 0.93	110.83 ± 1.73	112.19 ± 1.65	132.86 ± 2.16	64.12 ± 0.95	79.64 ± 1.28	...
3733 He I	2.21 ± 0.13	3.72 ± 0.23	...	...	...	...	...
3734 H13	1.62 ± 0.10	2.73 ± 0.17	1.41 ± 0.27	1.66 ± 0.33	1.39 ± 0.07	1.72 ± 0.09	2.41
3750 H12	1.72 ± 0.05	3.35 ± 0.13	1.56 ± 0.24	4.95 ± 0.99	2.28 ± 0.12	3.35 ± 0.24	3.07
3771 H11	2.20 ± 0.06	4.12 ± 0.14	2.29 ± 0.34	5.87 ± 1.06	2.66 ± 0.12	3.80 ± 0.24	4.00
3798 H10	3.11 ± 0.05	5.56 ± 0.13	3.18 ± 0.17	6.87 ± 0.52	3.92 ± 0.18	5.29 ± 0.29	5.34
3820 He I	0.56 ± 0.02	0.90 ± 0.03	0.11 ± 0.08	0.12 ± 0.10	...	...	...
3835 H9	4.66 ± 0.07	7.91 ± 0.15	4.31 ± 0.15	8.03 ± 0.44	5.84 ± 0.13	7.57 ± 0.23	7.37
3869 [Ne III]	19.07 ± 0.27	29.96 ± 0.46	27.21 ± 0.45	31.38 ± 0.56	39.79 ± 0.59	47.93 ± 0.76	...
3889 He I + H8	12.07 ± 0.17	19.22 ± 0.31	11.65 ± 0.24	16.54 ± 0.48	16.52 ± 0.26	20.29 ± 0.37	10.60
3967 [Ne III]	6.08 ± 0.17	9.08 ± 0.26	6.25 ± 0.29	7.08 ± 0.34	11.05 ± 0.17	13.04 ± 0.21	...
3970 H7	10.11 ± 0.16	15.10 ± 0.25	11.20 ± 0.34	12.69 ± 0.40	12.50 ± 0.22	14.74 ± 0.27	16.00
4026 He I	1.10 ± 0.02	1.60 ± 0.04	0.74 ± 0.17	0.82 ± 0.20	1.20 ± 0.10	1.40 ± 0.11	...
4068 [S II]	1.52 ± 0.03	2.15 ± 0.05	5.15 ± 0.26	5.73 ± 0.30	0.84 ± 0.06	0.98 ± 0.07	...
4076 [S II]	0.45 ± 0.02	0.64 ± 0.03	...	...	...	...	...
4101 Hδ	19.53 ± 0.28	27.69 ± 0.42	21.93 ± 0.35	26.89 ± 0.53	22.61 ± 0.35	26.36 ± 0.44	26.10
4177 [Fe II]	0.20 ± 0.05	0.27 ± 0.07	...	...	...	...	...
4233 Fe II	0.18 ± 0.04	0.23 ± 0.05	2.03 ± 0.23	2.20 ± 0.25	...	...	...
4244 [Fe II]	0.29 ± 0.03	0.38 ± 0.04	4.32 ± 0.21	4.66 ± 0.24	...	...	...
4277 O II+[Fe II]	0.19 ± 0.02	0.24 ± 0.03	3.44 ± 0.21	3.69 ± 0.23	...	...	...
4287 [Fe II]	0.48 ± 0.03	0.61 ± 0.04	4.80 ± 0.20	5.14 ± 0.22	0.24 ± 0.03	0.26 ± 0.04	...
4340 Hγ	39.69 ± 0.56	49.92 ± 0.73	40.96 ± 0.62	46.08 ± 0.77	42.59 ± 0.63	47.00 ± 0.71	47.10
4353 [Fe II]	0.05 ± 0.02	0.06 ± 0.03	1.48 ± 0.16	1.56 ± 0.17	...	...	...
4359 [Fe II]	0.53 ± 0.05	0.66 ± 0.06	4.24 ± 0.26	4.49 ± 0.28	...	...	...
4363 [O III]	1.98 ± 0.04	2.45 ± 0.05	2.80 ± 0.31	2.96 ± 0.34	8.80 ± 0.15	9.59 ± 0.17	...
4387 He I	0.30 ± 0.03	0.36 ± 0.04	...	...	...	...	...
4414 [Fe II]+O II	0.66 ± 0.06	0.80 ± 0.07	4.87 ± 0.52	5.11 ± 0.56	...	...	...
4452 [Fe II]	0.28 ± 0.05	0.34 ± 0.06	1.87 ± 0.22	1.95 ± 0.23	...	...	...
4458 [Fe II]	0.20 ± 0.04	0.23 ± 0.05	...	...	...	...	...
4471 He I	3.40 ± 0.06	4.00 ± 0.07	4.04 ± 0.63	4.20 ± 0.68	3.22 ± 0.09	3.44 ± 0.10	...
4475 [Fe II]	0.23 ± 0.05	0.27 ± 0.06	3.24 ± 0.30	3.37 ± 0.32	...	...	...
4493 [Fe II]	0.20 ± 0.03	0.23 ± 0.04	1.06 ± 0.15	1.10 ± 0.16	...	...	...
4515 [Fe II]	0.13 ± 0.02	0.15 ± 0.03	...	...	...	...	...
4563 [Cr III]?	0.09 ± 0.01	0.10 ± 0.02	...	...	...	...	...
4571 Mg I	0.15 ± 0.02	0.16 ± 0.03	...	...	...	...	...
4584 Fe II	0.15 ± 0.02	0.17 ± 0.02	1.84 ± 0.15	1.88 ± 0.16	...	...	...
4597 [Co IV]?	0.09 ± 0.02	0.10 ± 0.02	...	...	...	...	...
4607 N II+[Fe III]	0.14 ± 0.02	0.15 ± 0.03	...	...	...	...	...
4630 N II	0.30 ± 0.03	0.33 ± 0.04	1.87 ± 0.16	1.90 ± 0.16	...	...	...
4640 N III	0.19 ± 0.04	0.21 ± 0.04	...	...	...	...	...
4658 [Fe III]	1.51 ± 0.03	1.64 ± 0.04	3.36 ± 0.21	3.39 ± 0.21	0.99 ± 0.05	1.03 ± 0.05	...

Table 1. continued.

	Galaxy						
	Haro 11B		Haro 11C		ESO 338-IG 004		theory
Ion	$F(\lambda)/F(\mathrm{H}\beta)^a$	$I(\lambda)/I(\mathrm{H}\beta)^b$	$F(\lambda)/F(\mathrm{H}\beta)^a$	$I(\lambda)/I(\mathrm{H}\beta)^b$	$F(\lambda)/F(\mathrm{H}\beta)^a$	$I(\lambda)/I(\mathrm{H}\beta)^b$	Case B^c
4686 He II	0.91 ± 0.06	0.98 ± 0.07	...	...	2.15 ± 0.06	2.21 ± 0.07	...
4702 [Fe III]	0.34 ± 0.03	0.36 ± 0.04	...	...	0.26 ± 0.04	0.26 ± 0.04	...
4712 [Ar IV] + He I	0.67 ± 0.03	0.71 ± 0.04	...	...	0.90 ± 0.07	0.92 ± 0.07	...
4728 [Fe II]	0.16 ± 0.03	0.17 ± 0.03	...	...	...	...	...
4740 [Ar IV]	0.17 ± 0.01	0.17 ± 0.02	...	...	0.83 ± 0.07	0.84 ± 0.07	...
4755 [Fe III]	0.36 ± 0.03	0.37 ± 0.03	...	...	...	...	...
4770 [Fe III]	0.14 ± 0.02	0.14 ± 0.02	...	...	...	...	...
4778 [Fe III]	0.15 ± 0.03	0.15 ± 0.03	...	...	...	...	...
4814 [Fe II]	0.27 ± 0.02	0.28 ± 0.02	2.06 ± 0.16	2.03 ± 0.16	...	...	...
4861 Hβ	100.00 ± 1.42	100.00 ± 1.44	100.00 ± 1.45	100.00 ± 1.50	100.00 ± 1.45	100.00 ± 1.46	100.00
4881 [Fe III]	0.47 ± 0.02	0.47 ± 0.02	...	...	0.53 ± 0.04	0.53 ± 0.04	...
4890 [Fe II]	0.16 ± 0.01	0.16 ± 0.02	1.14 ± 0.10	1.11 ± 0.10	...	...	...
4905 [Fe II]	0.13 ± 0.01	0.13 ± 0.01	1.30 ± 0.14	1.26 ± 0.14	0.25 ± 0.02	0.25 ± 0.02	...
4922 He I	1.15 ± 0.03	1.12 ± 0.03	...	...	0.63 ± 0.05	0.62 ± 0.05	...
4930 [Fe III]	0.20 ± 0.03	0.19 ± 0.03	...	...	...	...	...
4943 O II	0.09 ± 0.02	0.09 ± 0.02	...	...	...	...	...
4959 [O III]	124.43 ± 1.76	119.38 ± 1.72	102.66 ± 1.49	99.02 ± 1.48	171.17 ± 2.46	167.96 ± 2.44	...
4986 [Fe III]	0.61 ± 0.02	0.58 ± 0.02	1.36 ± 0.20	1.31 ± 0.20	1.25 ± 0.05	1.22 ± 0.05	...
5007 [O III]	394.68 ± 5.59	371.56 ± 5.34	331.11 ± 4.76	317.19 ± 4.68	531.05 ± 7.61	517.00 ± 7.47	...
5016 He I	1.38 ± 0.03	1.29 ± 0.03	2.32 ± 0.22	2.22 ± 0.22	1.78 ± 0.06	1.73 ± 0.06	...
5041 Si II	0.25 ± 0.03	0.23 ± 0.03	...	...	...	...	...
5048 He I	0.13 ± 0.02	0.12 ± 0.02	...	...	...	...	...
5056 Si II	0.41 ± 0.03	0.37 ± 0.03	...	...	...	...	...
5159 [Fe II]	0.65 ± 0.02	0.58 ± 0.02	5.66 ± 0.19	5.31 ± 0.18	...	...	...
5169 Fe II	0.14 ± 0.02	0.12 ± 0.01	1.53 ± 0.14	1.43 ± 0.13	...	...	...
5199 [N I]	1.79 ± 0.03	1.57 ± 0.03	4.83 ± 0.17	4.50 ± 0.17	0.50 ± 0.05	0.47 ± 0.05	...
5220 [Fe II]	0.14 ± 0.04	0.12 ± 0.03	...	...	...	...	...
5235 Fe II?	0.19 ± 0.03	0.17 ± 0.02	1.28 ± 0.13	1.19 ± 0.13	...	...	...
5262 [Fe II]	0.29 ± 0.02	0.25 ± 0.01	1.68 ± 0.12	1.55 ± 0.11	...	...	...
5270 [Fe III]	1.06 ± 0.03	0.90 ± 0.02	2.82 ± 0.12	2.60 ± 0.12	0.58 ± 0.04	0.54 ± 0.03	...
5273 [Fe II]	0.22 ± 0.01	0.18 ± 0.01	2.52 ± 0.11	2.33 ± 0.11	...	...	...
5317 Fe II?	0.26 ± 0.02	0.21 ± 0.01	3.26 ± 0.18	2.99 ± 0.17	...	...	...
5334 [Fe II]	0.21 ± 0.03	0.17 ± 0.03	1.78 ± 0.14	1.63 ± 0.13	...	...	...
5363 [Ni IV]	0.17 ± 0.06	0.14 ± 0.05	1.23 ± 0.26	1.12 ± 0.24	...	...	...
5376 [Fe II]	0.20 ± 0.03	0.17 ± 0.02	2.09 ± 0.29	1.91 ± 0.27	...	...	...
5518 [Cl III]	0.38 ± 0.03	0.29 ± 0.02	0.86 ± 0.13	0.77 ± 0.12	...	...	...
5535 Fe II? N II? C II?	0.12 ± 0.08	0.09 ± 0.06	...	...	...	...	...
5538 [Cl III]	0.26 ± 0.02	0.20 ± 0.01	...	...	...	...	...
5755 [N II]	1.62 ± 0.03	1.16 ± 0.02	6.04 ± 0.18	5.25 ± 0.16	...	...	...
5876 He I	19.52 ± 0.29	13.50 ± 0.21	16.12 ± 0.47	13.81 ± 0.42	13.16 ± 0.23	11.27 ± 0.20	...
5958 Si II	0.16 ± 0.02	0.08 ± 0.01	...	...	...	...	...
5979 Si II	0.36 ± 0.03	0.24 ± 0.02	...	...	...	...	...
6046 O I	0.13 ± 0.04	0.09 ± 0.02	...	...	...	...	...
6300 [O I]	6.67 ± 0.10	4.06 ± 0.07	9.55 ± 0.27	7.81 ± 0.23	2.95 ± 0.09	2.39 ± 0.07	...
6312 [S III]	1.82 ± 0.05	1.10 ± 0.03	1.28 ± 0.21	1.05 ± 0.18	1.62 ± 0.08	1.32 ± 0.06	...
6347 Si II	0.47 ± 0.02	0.28 ± 0.02	...	...	...	...	...
6364 [O I]	2.36 ± 0.04	1.41 ± 0.02	2.69 ± 0.12	2.18 ± 0.10	0.66 ± 0.10	0.53 ± 0.08	...
6365 [Ni II]	0.16 ± 0.02	0.09 ± 0.01	...	...	...	...	...
6371 Si II	0.30 ± 0.02	0.18 ± 0.01	...	...	...	...	...
6384 Fe II	0.19 ± 0.04	0.11 ± 0.02	...	...	...	...	...
6456 Fe II	0.25 ± 0.04	0.15 ± 0.02	1.00 ± 0.13	0.81 ± 0.10	...	...	...
6516 Fe II	0.12 ± 0.02	0.07 ± 0.01	...	...	...	...	...
6548 [N II]	28.91 ± 0.41	16.38 ± 0.26	22.86 ± 0.38	18.22 ± 0.33	2.91 ± 0.07	2.29 ± 0.06	...
6563 Hα^d	514.82 ± 7.29	290.71 ± 4.53	358.69^d ± 5.17	286.36^d ± 4.60	374.18 ± 5.37	294.56 ± 4.62	282.00
6583 [N II]	86.96 ± 1.26	48.81 ± 0.78	72.57 ± 1.06	57.64 ± 0.94	9.04 ± 0.15	7.10 ± 0.13	...
6667 [Ni II]	0.18 ± 0.03	0.10 ± 0.02	...	...	...	...	...
6678 He I	6.36 ± 0.09	3.48 ± 0.06	3.50 ± 0.10	2.75 ± 0.08	3.90 ± 0.08	3.03 ± 0.07	...

Table 1. continued.

	Galaxy						
	Haro 11B		Haro 11C		ESO 338-IG 004		theory
Ion	$F(\lambda)/F(\mathrm{H}\beta)^a$	$I(\lambda)/I(\mathrm{H}\beta)^b$	$F(\lambda)/F(\mathrm{H}\beta)^a$	$I(\lambda)/I(\mathrm{H}\beta)^b$	$F(\lambda)/F(\mathrm{H}\beta)^a$	$I(\lambda)/I(\mathrm{H}\beta)^b$	Case B^c
6716 [S II]	28.86 ± 0.41	15.63 ± 0.25	37.16 ± 0.55	29.14 ± 0.48	14.07 ± 0.22	10.88 ± 0.18	...
6731 [S II]	18.99 ± 0.27	10.25 ± 0.16	17.08 ± 0.27	13.37 ± 0.24	10.99 ± 0.17	8.49 ± 0.15	...
7002 O I	0.09 ± 0.01	0.04 ± 0.00	...	...	...	...	...
7065 He I	6.73 ± 0.10	3.34 ± 0.06	3.98 ± 0.09	3.02 ± 0.07	3.84 ± 0.07	2.87 ± 0.06	...
7136 [Ar III]	14.37 ± 0.21	7.01 ± 0.12	10.49 ± 0.26	7.92 ± 0.21	7.56 ± 0.13	5.60 ± 0.11	...
7155 [Fe II]	0.55 ± 0.03	0.27 ± 0.01	1.76 ± 0.22	1.32 ± 0.17	...	...	...
7172 [Fe II]	0.14 ± 0.02	0.07 ± 0.01	...	...	...	...	...
7236 C II	0.19 ± 0.01	0.09 ± 0.01	...	...	...	...	...
7254 O I	0.31 ± 0.02	0.15 ± 0.01	...	...	...	...	...
7281 He I	0.94 ± 0.02	0.44 ± 0.01	...	...	0.68 ± 0.04	0.50 ± 0.03	...
7291 [Ca II]	0.19 ± 0.02	0.09 ± 0.01	...	...	...	...	...
7320 [O II]	5.32 ± 0.08	2.49 ± 0.04	3.47 ± 0.10	2.58 ± 0.08	2.42 ± 0.06	1.76 ± 0.04	...
7330 [O II]	4.38 ± 0.06	2.04 ± 0.03	2.35 ± 0.11	1.74 ± 0.09	2.08 ± 0.05	1.51 ± 0.04	...
7378 [Ni II]	0.67 ± 0.02	0.31 ± 0.01	1.66 ± 0.12	1.23 ± 0.09	...	...	...
7412 [Ni II]	0.15 ± 0.02	0.07 ± 0.01	0.44 ± 0.09	0.32 ± 0.07	...	...	...
7711 Fe II	0.08 ± 0.01	0.03 ± 0.00	...	...	...	...	...
7751 [Ar III]	3.56 ± 0.05	1.52 ± 0.03	1.30 ± 0.10	0.94 ± 0.07	1.90 ± 0.05	1.33 ± 0.04	...
7816 He I	0.10 ± 0.02	0.04 ± 0.01	...	...	...	...	...
8125 [Cr II]	0.23 ± 0.02	0.09 ± 0.01	...	...	...	...	...
8188 N I	0.37 ± 0.03	0.14 ± 0.01	...	...	...	...	...
8216 N I	0.42 ± 0.06	0.16 ± 0.02	...	...	...	...	...
8223 N I?	0.41 ± 0.03	0.16 ± 0.01	...	...	...	...	...
8229 Fe II	0.26 ± 0.03	0.10 ± 0.01	...	...	...	...	...
8242 N I	0.27 ± 0.02	0.10 ± 0.01	...	...	...	...	...
8299 P28	0.09 ± 0.01	0.03 ± 0.00	...	...	...	...	0.08
8306 P27	0.14 ± 0.01	0.05 ± 0.01	...	...	...	...	0.09
8314 P26	0.09 ± 0.01	0.03 ± 0.00	...	...	...	...	0.10
8323 P25	0.16 ± 0.01	0.06 ± 0.00	...	...	...	...	0.12
8334 P24	0.31 ± 0.02	0.12 ± 0.01	...	...	0.26 ± 0.03	0.18 ± 0.02	0.13
8345 P23	0.27 ± 0.02	0.10 ± 0.01	...	...	0.26 ± 0.04	0.18 ± 0.03	0.15
8359 P22	0.51 ± 0.01	0.19 ± 0.01	...	...	0.37 ± 0.05	0.25 ± 0.03	0.17
8374 P21	0.37 ± 0.01	0.14 ± 0.00	...	...	0.26 ± 0.04	0.17 ± 0.03	0.19
8392 P20	0.40 ± 0.01	0.15 ± 0.00	...	...	0.37 ± 0.04	0.25 ± 0.03	0.22
8413 P19	0.45 ± 0.01	0.17 ± 0.00	...	...	0.35 ± 0.04	0.24 ± 0.03	0.26
8438 P18	0.64 ± 0.01	0.24 ± 0.01	...	...	0.37 ± 0.03	0.25 ± 0.02	0.31
8446 O I	3.93 ± 0.06	1.47 ± 0.03	7.34 ± 0.16	5.03 ± 0.12	0.74 ± 0.04	0.49 ± 0.03	...
8470 P17	0.62 ± 0.01	0.23 ± 0.01	...	...	0.36 ± 0.04	0.24 ± 0.03	0.36
8490 Fe II	0.19 ± 0.01	0.07 ± 0.01	...	...	...	...	...
8505 P16	0.76 ± 0.02	0.28 ± 0.01	...	...	0.41 ± 0.03	0.27 ± 0.02	0.44
8548 P15	0.90 ± 0.02	0.33 ± 0.01	...	...	0.37 ± 0.04	0.24 ± 0.02	0.53
8579?	0.31 ± 0.02	0.11 ± 0.01	...	...	...	...	...
8601 P14	1.25 ± 0.02	0.46 ± 0.01	...	...	0.70 ± 0.04	0.46 ± 0.03	0.65
8617 [Fe II]	0.52 ± 0.02	0.19 ± 0.01	...	...	...	...	...
8667 P13	1.68 ± 0.03	0.60 ± 0.01	...	...	0.76 ± 0.04	0.50 ± 0.03	0.81
8683 N I	0.48 ± 0.02	0.17 ± 0.01	...	...	...	...	...
8753 P12	2.19 ± 0.04	0.78 ± 0.02	0.81 ± 0.06	0.55 ± 0.04	1.23 ± 0.08	0.80 ± 0.05	1.04
8865 P11	2.81 ± 0.04	0.98 ± 0.02	...	...	1.62 ± 0.05	1.04 ± 0.03	1.35
9017 P10	3.66 ± 0.06	1.24 ± 0.02	...	...	2.13 ± 0.05	1.35 ± 0.04	1.80
9069 [S III]	46.14 ± 0.65	15.58 ± 0.29	21.14 ± 0.33	14.43 ± 0.29	15.17 ± 0.23	9.68 ± 0.19	...
9095 Ca I]	0.19 ± 0.02	0.06 ± 0.01	...	...	...	...	...
9231 P9	6.11 ± 0.10	2.01 ± 0.04	...	...	1.42^e ± 0.07	0.89^e ± 0.04	2.49
9464 He I	0.37 ± 0.02	0.12 ± 0.01	...	...	...	...	...
9532 [S III]	136.72 ± 1.94	43.16 ± 0.82	59.08 ± 0.86	38.54 ± 0.76	41.96 ± 0.62	25.96 ± 0.50	...
9548 Pe	10.08 ± 0.15	3.17 ± 0.06	3.26 ± 0.12	2.10 ± 0.08	3.51 ± 0.09	2.17 ± 0.06	3.57
9850 [C I]	0.57 ± 0.06	0.17 ± 0.02	...	...	...	...	...

b) NIR range

Table 1. continued.

Ion	Galaxy						theory
	Haro 11B		Haro 11C		ESO 338-IG 004		
	$F(\lambda)/F(\mathrm{H}\beta)^a$	$I(\lambda)/I(\mathrm{H}\beta)^b$	$F(\lambda)/F(\mathrm{H}\beta)^a$	$I(\lambda)/I(\mathrm{H}\beta)^b$	$F(\lambda)/F(\mathrm{H}\beta)^a$	$I(\lambda)/I(\mathrm{H}\beta)^b$	Case B[c]
10050 Pd	...	...	...	...	9.56 ± 0.32	5.75 ± 0.21	5.40
10432 [Fe II]?	0.18 ± 0.06	0.05 ± 0.02	...	...	...	...	...
10502 Fe II	0.40 ± 0.04	0.11 ± 0.01	1.94 ± 0.22	1.20 ± 0.14	...	...	...
10551?	0.27 ± 0.03	0.07 ± 0.01	...	...	...	...	...
10715 [Ni II]	0.21 ± 0.04	0.06 ± 0.01	...	...	...	...	...
10829 He I	120.40 ± 1.71	32.64 ± 0.66	46.44 ± 0.76	28.33 ± 0.63	47.85 ± 2.23	27.75 ± 1.36	...
10910 He I	1.58 ± 0.11	0.42 ± 0.03	...	...	...	...	...
10941 Pγ	20.45[e] ± 0.32	5.48[e] ± 0.12	8.40[e] ± 0.38	5.10[e] ± 0.25	13.90 ± 0.25	8.03 ± 0.18	8.77
11287 O I+Fe II	1.74 ± 0.10	0.45 ± 0.03	...	...	...	...	...
11620 H_2	0.18 ± 0.04	0.05 ± 0.01	...	...	...	...	...
11850 H_2	0.19 ± 0.04	0.05 ± 0.01	...	...	...	...	...
11880 H_2+[Fe II]?	0.83 ± 0.05	0.20 ± 0.01	...	...	...	...	...
11970 He I	0.51 ± 0.05	0.13 ± 0.01	...	...	...	...	...
12070 H_2	0.09 ± 0.03	0.02 ± 0.01	...	...	...	...	...
12289 N I	0.15 ± 0.03	0.04 ± 0.01	...	...	...	...	...
12330 H_2	0.52 ± 0.04	0.13 ± 0.01	...	...	...	...	...
12380 H_2+Fe II?	0.19 ± 0.03	0.04 ± 0.01	...	...	...	...	...
12525?	0.90 ± 0.04	0.21 ± 0.01	...	...	...	...	...
12570 [Fe II]	6.14 ± 0.11	1.44 ± 0.03	4.77 ± 0.22	2.77 ± 0.14	...	...	...
12790 He I	3.83 ± 0.07	0.89 ± 0.02	2.77 ± 0.19	1.59 ± 0.12	0.88 ± 0.05	0.48 ± 0.03	...
12821 Pβ	62.09 ± 0.88	14.36 ± 0.31	30.54 ± 0.53	17.59 ± 0.42	27.22 ± 0.42	14.78 ± 0.33	15.70
13165 O I	0.92 ± 0.10	0.21 ± 0.02	...	...	...	...	...
14967 Br25	0.34 ± 0.03	0.07 ± 0.01	...	...	...	...	0.06
15005 Br24	0.28 ± 0.03	0.06 ± 0.01	...	...	...	...	0.06
15043 Br23	0.25 ± 0.02	0.05 ± 0.00	...	...	...	...	0.07
15087 Br22	0.34 ± 0.03	0.07 ± 0.01	...	...	...	...	0.08
15137 Br21	0.35 ± 0.03	0.07 ± 0.01	...	...	...	...	0.09
15196 Br20	0.50 ± 0.03	0.10 ± 0.01	...	...	...	...	0.11
15265 Br19	0.40 ± 0.02	0.08 ± 0.01	...	...	...	...	0.12
15346 Br18	1.19 ± 0.04	0.24 ± 0.01	...	...	...	...	0.15
15443 Br17	1.12 ± 0.05	0.23 ± 0.01	...	...	...	...	0.18
15530?	0.33 ± 0.03	0.07 ± 0.01	...	...	...	...	...
15561 Br16	1.05 ± 0.07	0.21 ± 0.01	...	...	...	...	0.21
15705 Br15	1.29 ± 0.05	0.26 ± 0.01	...	...	...	...	0.26
15885 Br14	1.49 ± 0.04	0.30 ± 0.01	...	...	0.44 ± 0.05	0.22 ± 0.03	0.31
16010 H_2	0.10 ± 0.03	0.02 ± 0.01	...	...	...	...	...
16114 Br13	2.08 ± 0.04	0.42 ± 0.01	...	...	0.71 ± 0.04	0.36 ± 0.02	0.39
16410 Br12	2.24 ± 0.05	0.44 ± 0.01	...	...	0.77 ± 0.04	0.39 ± 0.02	0.50
16436 [Fe II]	6.28 ± 0.10	1.25 ± 0.03	3.14 ± 0.18	1.71 ± 0.11	...	...	...
16640 [Fe II]	0.22 ± 0.05	0.04 ± 0.01	...	...	...	...	...
16769 [Fe II]	0.36 ± 0.03	0.07 ± 0.01	...	...	...	...	...
16811 Br11	3.51 ± 0.06	0.69 ± 0.02	...	...	1.02 ± 0.08	0.52 ± 0.04	0.65
16873 Fe II	0.40 ± 0.03	0.08 ± 0.01	...	...	...	...	...
17006 He I	1.16 ± 0.03	0.23 ± 0.01	...	...	0.55 ± 0.04	0.28 ± 0.02	...
17367 Br10	5.10 ± 0.08	0.99 ± 0.02	2.60 ± 0.37	1.41 ± 0.20	1.92 ± 0.06	0.97 ± 0.03	0.87
18179 Br9	7.44[e] ± 0.31	1.42[e] ± 0.06	...	...	...	...	1.21
18693?	9.90 ± 0.34	1.88 ± 0.07	...	...	...	...	...
18756 Pα	42.33[e] ± 0.77	8.02[e] ± 0.21	...	...	13.11[e] ± 0.23	6.55[e] ± 0.16	31.90
19450 Brδ	10.06 ± 0.17	1.89 ± 0.05	2.63 ± 0.22	1.40 ± 0.12	1.18 ± 0.09	0.59 ± 0.05	1.73
19540 He I+[Fe II]	0.73 ± 0.07	0.14 ± 0.01	...	...	...	...	...
19570 H_2	0.61 ± 0.03	0.11 ± 0.01	...	...	0.58 ± 0.07	0.29 ± 0.03	...
20340 H_2	0.40 ± 0.08	0.07 ± 0.02	...	...	...	...	...
20586 He I	8.22 ± 0.13	1.52 ± 0.04	1.48 ± 0.14	0.79 ± 0.08	2.02 ± 0.09	1.00 ± 0.05	...
20730 H_2	0.33 ± 0.03	0.06 ± 0.01	...	...	...	...	...
20888 Fe II	0.19 ± 0.03	0.04 ± 0.01	...	...	...	...	...
21130 He I	0.57 ± 0.04	0.11 ± 0.01	...	...	...	...	...

Table 1. continued.

	Galaxy						
	Haro 11B		Haro 11C		ESO 338-IG 004		theory
Ion	$F(\lambda)/F(\mathrm{H}\beta)^a$	$I(\lambda)/I(\mathrm{H}\beta)^b$	$F(\lambda)/F(\mathrm{H}\beta)^a$	$I(\lambda)/I(\mathrm{H}\beta)^b$	$F(\lambda)/F(\mathrm{H}\beta)^a$	$I(\lambda)/I(\mathrm{H}\beta)^b$	Case B[c]
21220 H_2	1.21 ± 0.03	0.22 ± 0.01	...	...	0.56 ±0.06	0.28 ±0.03	...
21620 He I	0.42 ± 0.04	0.08 ± 0.01	...	...	...	...	...
21661 Brγ	16.73 ± 0.24	3.07 ± 0.07	5.38 ± 0.19	2.85 ± 0.12	5.03 ± 0.12	2.48 ± 0.07	2.63
22181?	0.37 ± 0.04	0.07 ± 0.01	...	...	...	...	...
22230 H_2	0.26 ± 0.05	0.05 ± 0.01	...	...	...	...	...
22480 H_2	0.20 ± 0.04	0.04 ± 0.01	...	...	...	...	...
			c) MIR range[f]				
10.51μm[S IV]	12.76 ± 0.10	...	...	...	...	...	...
12.81μm[Ne II]	9.07 ± 0.14	...	...	...	...	...	...
15.55μm[Ne III]	28.51 ± 0.40	...	...	...	...	...	...
18.71μm[S III]	13.14 ± 0.12	...	...	...	...	...	...
$C(\mathrm{H}\beta)$	0.74		0.27		0.31		
$F(\mathrm{H}\beta)^g$	344.20		63.59		121.40		
EW(abs) Å	0.20		0.35		0.15		

Notes. [(a)] $F(\lambda)$ is observed flux, $F(\lambda)/F(\mathrm{H}\beta)$ ratio designations with ×100. [(b)] $I(\lambda)$ is extinction-corrected flux, $I(\lambda)/I(\mathrm{H}\beta)$ ratio designations with ×100. [(c)] Hydrogen recombination-line relative intensities by Hummer & Storey (1987). [(d)] The observed flux of Hα in Haro 11C is $F(\mathrm{H}\alpha) = 3.350 \times 10^{-14}$ erg s^{-1} cm^{-2}. In this Table we show the $F(\mathrm{H}\alpha)/F(\mathrm{H}\beta)$ ratio corresponding to $F(\mathrm{H}\alpha) = 2.281 \times 10^{-14}$ erg s^{-1} cm^{-2} obtained after subtraction of the P Cyg component. [(e)] Affected by the telluric absorption. [(f)] $F(\lambda)/F(\mathrm{H}\beta)$ ratio from Wu et al. (2008). [(g)] In units of 10^{-16} erg s^{-1} cm^{-2}.